The effect of blade aerodynamic modelling on the prediction of the blade airloads and the acoustic signature of the HART II rotor

Mary E. Kelly* and Richard E. Brown†

mkelly@aero.gla.ac.uk, rbrown@aero.gla.ac.uk
Department of Aerospace Engineering
University of Glasgow,
Glasgow, G12 8QQ.

ABSTRACT

As a rotorcraft descends or manoeuvres, the interactions which occur between the rotor blades and vortical structures within the rotor wake produce highly impulsive loads on the blades and with these a highly intrusive external noise. Brown's Vorticity Transport Model has been used to investigate the influence of the fidelity of the local blade aerodynamic model on the quality of the prediction of the high-frequency airloads associated with blade-vortex interactions and thus on the accuracy with which the acoustic signature of the aircraft can be predicted. The Vorticity Transport Model can resolve very accurately the structure of the wake, and allows significant flexibility in the way that the blade loading can be represented. The predictions of two models for the local blade aerodynamics are compared for all three of the HART II flight cases. The first model is a simple lifting-line model and the second is a somewhat more sophisticated lifting-chord model based on unsteady thin aerofoil theory. A marked improvement in accuracy of the predicted high-frequency airloads and acoustic signature of the HART II rotor is obtained when the lifting-chord model for the blade aerodynamics is used instead of the lifting-line type approach. Errors in the amplitude and phase of the loading peaks are reduced and the quality of the prediction is affected to a lesser extent by the computational resolution of the wake. Predictions of the acoustic signature of the rotor are similarly affected, with the lifting-chord model at the highest resolution producing the best representation of the distribution of sound pressure on the ground plane below the rotor.

NOMENCLATURE

a_{ij}	Interpolation coefficients
b	Blade semi-chord
c	Blade chord, $c = 2b$
C_N	Section normal force coefficient
C_T	Rotor thrust coefficient, $T/\rho A(\Omega R)^2$
f	Reverse flow parameter
$F_j(\psi)$	Azimuthal interpolation functions
K	Coefficient of integration
M	Mach number, $M = U_\infty/a$
N_a	Number of azimuthal interpolation functions
N_r	Number of radial interpolation functions
$P_i(r)$	Radial interpolation functions
r	Blade spanwise coordinate scaled by R
R	Rotor radius
S	Local vorticity source
t	Time
$\mathbf{u}$	Flow velocity vector
U_∞	Magnitude of the freestream velocity
w	Blade velocity relative to background flow
x	Aerofoil chordwise coordinate, $x = b\cos\varphi$
X	Rotor streamwise coordinate
Y	Rotor lateral coordinate
y_{el}	Elastic lag motion
Z	Rotor vertical coordinate
z_{el}	Elastic flap motion
φ	Glauert's variable
Γ	Total bound circulation
λ	Velocity due to the vorticity in the flow
ν	Viscosity of the fluid
θ_{el}	Elastic blade torsion
ρ	Density of the fluid
τ	Unit vector parallel to blade trailing edge
ψ	Azimuth angle
ω	Vorticity in the flow

*Postgraduate Research Student
†Mechan Chair of Engineering

Presented at the 35th European Rotorcraft Forum, Hamburg, Germany, 22–50 Sept. 2009.

1 INTRODUCTION

The aerodynamic environment in which a rotorcraft operates is dominated by the strong vortical structures that are generated by the rotating blade system. The interaction between these vortices and the various structural components of the aircraft accounts for many of the design problems which rotorcraft encounter. In particular, the localised aerodynamic interactions between the rotor blades and the vortices that they produce, known as blade vortex interactions (BVIs), produce highly impulsive loads along the blade span and are a significant source of noise and vibration. The intensity and directivity of the noise generated by a helicopter is of considerable importance for both civilian and military applications as strict certification and community noise constraints often apply. Such requirements have led industry to investigate the sources of noise associated with helicopters in flight with the aim of significantly reducing current noise levels.

To predict accurately the noise produced by a particular design of aircraft it is essential to first accurately determine the position, amplitude and strength of the BVI-induced loading perturbations on the rotor blades. This process requires the accurate determination of both the position and strength of the vortical structures in the wake and also the correct position and deformation of the rotor blades. The complexity of the rotor wake, and the strong mutual dependence of the aerodynamics and structural dynamics of the blades, renders accurate prediction of the BVI-related blade airloads a particularly challenging task. A tool that can predict accurately the high frequency components of the blade loading, particularly those that are responsible for the rather objectionable characteristics of the helicopter under certain flight conditions, would be of significant benefit to the designers of modern rotorcraft in the drive to reduce noise.

The Higher Harmonic Control Aeroacoustics Rotor Test (HART) programme [1–4] was initiated to provide experimental insight into the structure of the rotor wake, the effect of the wake on the aerodynamic loading on the rotor blades and, thus, on the acoustic signature of the rotor. The rotor that was used in this programme was a scaled model of that used on the Bo105 helicopter. The HART II experiment was designed specifically to replicate a descending flight condition in which the loading on the rotor was known to contain significant high-frequency content due to the presence of blade vortex interactions.

Computational Fluid Dynamics (CFD) calculations of the flow around the entire rotorcraft, or even just the rotor, are extremely challenging. Nevertheless, recent advances in coupling Rotorcraft Computational Structural Dynamic (CSD) analyses to Rotorcraft CFD have demonstrated significant progress in accurately predicting the rotor blade motion and capturing the associated blade airloads. Boyd [5], Lim *et al.* [6] and Lim and Strawn [7] show encouraging results in comparison to experimental data for their prediction of the BVI-induced airloads on the HART II rotor, for instance. For most CFD methods, the numerical dissipation which is inherent in the approach necessitates very high grid densities to maintain the fidelity of the wake, particularly if the structure of the wake is to be resolved to a level where the high frequency character of the BVI-generated airloads can be captured. At present this invariably results in solutions that are grid dependent given the prohibitive computational cost of rotor calculations on grids that are sufficiently fine to resolve the detailed structure of the wake.

There is a drive within the industry, particularly in the context of rotor design, to develop methods which can achieve high fidelity resolutions but at a much reduced computational cost when compared to CFD calculations of full helicopter configurations. One approach is via the so-called comprehensive code which couples structural and aerodynamics analysis to a flight dynamics model. Such an approach often uses lifting-line or lifting surface type aerodynamic models to provide blade airload information and a prescribed- or free-wake approach to portray the dynamics of the wake system. Often, though, comprehensive analyses require empirical corrections to portray accurately the unsteady aerodynamics within the flow field, and additional considerations are required to account for compressibility effects and stall. Lifting-line or lifting surface type aerodynamic models are relatively simple and easy to implement, but the physical accuracy of their response to the dynamics of the wake, especially if this is based on a prescribed- or free-wake approach, can be called into question especially in terms of resolving the detail of the close blade-wake encounters associated with BVI. It is often not clear whether discrepancies in the wake model, or instead in the blade aerodynamic model that lies at the source of the wake, are responsible for the deficiencies in prediction of the BVI-induced loads that appear to be characteristic of this type of approach.

The Vorticity Transport Model (VTM) is a comprehensive rotorcraft model in which the evolution of the wake is based on a time-dependent vorticity-velocity formulation of the Navier-Stokes equations, solved computationally on a structured grid system surrounding the rotor. This approach has been shown to yield a very accurate representation of the vortical structures within a rotor's wake, yet offers significant flexibility in the way that the source of vorticity into the wake can be generated. For instance, a simple lifting-line model for the blade aerodynamics can be used, or a full, primitive-variable CFD calculation of the blade flow can be embedded in the calculation [8]. This flexibility makes the VTM ideal for studying the effect of the blade aerodynamic model on the fidelity

of the prediction of the high-frequency, BVI-induced loads on the rotor.

The VTM framework has been used previously to predict the geometry of the wake system and the resultant rotor blade loading for the HART II rotor using a lifting-line model for the blade aerodynamics [9, 10] and in comparison to a lifting-chord model [11]. These earlier investigations suggested that accurate prediction of the high-harmonic, BVI-induced component of the airloads on the rotor is greatly influenced by the accuracy to which the wake geometry can be represented. Moreover, the high-frequency, BVI-induced component of the loading is very sensitive to the cell size that is used in the computations when a lifting-line model is used to represent the aerodynamic environment of the rotor blades. Sensitivity to the computational resolution that is used is reduced markedly when a lifting-chord model [11] is used in place of the lifting-line approach. Nevertheless, comparisons of the predicted wake structure and the trajectory of the vortices as they pass through the rotor disc have shown excellent agreement with the vortex core positions as measured during the HART II experiment regardless of the aerodynamic model that is used [9, 10].

The work presented in Ref. 11 focused on the aerodynamic issues involved in predicting the blade airloads and the rotor wake structure in regimes dominated by strong blade vortex interaction. In particular, the effect of the fidelity of the local model for the blade aerodynamics on the quality of the BVI-airload predictions was investigated. This paper extends that work by comparing the measured acoustic signature of the HART II rotor with that calculated from the airloads predicted by Brown's Vorticity Transport Model (VTM) when coupled to the two different approaches to modelling the local aerodynamics of the blades. This work aims to correlate the various features in the acoustic signal produced by the rotor to the specific features within the blade loading, and thus to refine our understanding of how the predictions of acoustic signature of the rotor are affected by the fidelity of the model that is used to predict its aerodynamic loading.

2 ROTOR MODEL

2.1 HART II Rotor

The model rotor used in the HART II test was based on that of the Bo105 main rotor. The rotor had four blades and was scaled both geometrically and aeroelastically to 40% of the full rotor size, giving a radius of 2m and a chord of 0.121m. The rotor blades had a NACA23012 aerofoil with the trailing edge modified to form a 5.4mm (4.46% chord) tab. The blades were rectangular with square tip and incorporated -8° of linear twist and a pre-cone angle of 2.5°.

The rotor was flown in descending flight at an advance ratio of 0.15 and a rotor shaft angle of 5.3°. This test point was selected as being analogous to the full-scale flight condition that yields maximum BVI noise radiation. The focus of the test was on three different flight cases – a baseline (BL) case with conventional control inputs, and two cases with higher harmonic control (HHC) inputs applied to the rotor at a frequency of three cycles per rotor revolution – the so-called minimum-vibration (MV) and minimum-noise (MN) cases. Further operational parameters for the test are summarised in Table 1. A detailed description of the rotor model and the measurement procedures used in the HART II test are given in Refs. 1–4.

Table 1: Rotor operational parameters

Forward velocity	33 m/s
Rotational speed	1041 rpm
Blade passage frequency	69.4 Hz
Shaft tilt	5.3°
Thrust coefficient	0.00457
Advance ratio	0.151

2.2 Computational Model

Simulations of the HART II test cases were performed using the Vorticity Transport Model (VTM). The present formulation of the VTM, developed by Brown and Line [12, 13] couples a model for the aerodynamics of the blade to an Eulerian representation of the dynamics of the vorticity in the flow field.

2.2.1 Wake Model

In the VTM, the vorticity in the flow field is evolved by solution of the Navier-Stokes equations in vorticity-velocity form on a structured Cartesian grid surrounding the rotor. Assuming incompressible flow with velocity $\mathbf{u}$, the associated vorticity distribution $\omega = \nabla \times \mathbf{u}$ evolves according to the unsteady vorticity transport equation

$$\frac{\partial}{\partial t}\omega + \mathbf{u} \cdot \nabla\omega - \omega \cdot \nabla\mathbf{u} = S + \nu\nabla^2\omega \qquad (1)$$

where ν is the viscosity of the fluid. In this formulation the vorticity then becomes the conserved variable within the flow and thus is not affected by the numerical dissipation which is inherent in CFD codes based on a pressure-velocity formulation of the Navier-Stokes equations. In addition, the local rate of numerical *diffusion* is controlled very effectively by using a set of highly compressive flux limiters within the particular implementation of Toro's Weighted Average Flux method [14] that is used within the code to convect

the solution through time. At each time step, the velocity at the cell faces is obtained from the vorticity distribution using a fast multipole technique to invert the differential form of the Biot-Savart equation

$$\nabla^2 \mathbf{u} = -\nabla \times \omega. \tag{2}$$

An adaptive grid is used to track the evolving vorticity in such a way that cells only exist in regions of the computational domain where the vorticity is non-zero. As the vorticity moves to a new location, new cells are created and any cells that no longer contain vorticity are destroyed. Thus, the grid structure is free to follow the evolution of the wake, eliminating the requirement for explicit numerical boundary conditions at the edge of the computational domain and increasing the computational efficiency of the method. Moreover, a nested grid system allows for fine resolution close to the rotor and then a systematic decrease in resolution with distance from the rotor hub.

2.2.2 Blade Aerodynamic Model

Two separate blade models have been incorporated within this VTM framework in order to yield the aerodynamic loading on the blades. Firstly, an extension of the Weissinger-L formulation of lifting-line theory is implemented on a series of discrete panels along the length of each rotor blade. A bound vortex is attached to the quarter-chord of each panel. The strength of the bound vorticity along the length of the blade is then determined by enforcing, simultaneously, a condition of zero through-flow at a set of collocation points that are located at the three-quarter chord of each panel.

A second model for the blade aerodynamics is based on an extension of classical unsteady thin aerofoil theory and uses a particular formulation for the airloads which is based on that developed in state-space form for flexible aerofoils by Peters *et al* [15].

The zero through-flow boundary condition allows the total bound circulation on the aerofoil to be written as

$$\Gamma = 2\pi b \left[f\left(w_0 - \lambda_0\right) + \frac{1}{2}\left(w_1 - \lambda_1\right) \right], \tag{3}$$

where f is a reverse flow parameter designed to enforce the Kutta condition at the downwind edge of the aerofoil. The circulation is defined in terms of the weighted integrals, given by

$$\lambda_n = \frac{1}{K_n} \int_0^\pi \lambda \cos^n \varphi \; d\varphi \tag{4}$$

and

$$w_n = \frac{1}{K_n} \int_0^\pi w \cos^n \varphi \; d\varphi, \tag{5}$$

where w is the component, normal to the blade chord, of the blade velocity relative to the uniform background flow and λ is the component, again normal to the blade chord, of the velocity due to all vorticity in the computational domain except that which is bound to the panel under consideration. Glauert's variable φ is defined such that

$$\begin{gathered} x = b\cos\varphi \\ -b \le x \le +b, \quad 0 \le \varphi \le \pi. \end{gathered} \tag{6}$$

and

$$K_n = \int_0^\pi \cos^n \varphi \; d\varphi \tag{7}$$

These integrals are evaluated numerically after evaluating the integrands at several discrete points along the chord of each blade panel. In all cases described in this paper these points were cosine-distributed along the chord to give enhanced resolution of the steep loading gradient near the leading edge of the blade.

The sectional lift (per unit span) is then given by

$$L_0 = \rho U_\infty \left(\Gamma + \frac{1}{2}\lambda_1 \right) + \pi \rho b^2 \left(\dot{w}_0 \right). \tag{8}$$

In all cases, forty panels in a cosine distribution were used to resolve the spanwise variation in loading along the length of the blade. In both aerodynamic models, the trailed and shed vorticity from each vortex panel is added to the near wake downstream of the blade as the local vorticity source

$$S = -\tau \frac{\partial \Gamma}{\partial t} + \mathbf{u}_b \frac{\partial \Gamma}{\partial r}, \tag{9}$$

where τ is the unit vector parallel to the trailing edge of the blade and $\mathbf{u}_b$ is the velocity of the trailing edge relative to the air. Most importantly in the present context, the shed vorticity distribution behind the blade is fully resolved using this approach. Its influence on the unsteady aerodynamic response of the system is thus captured directly in the simulations without the need to resort to empirical modelling of the indicial response of the blade, as is done in some comprehensive codes in order to compensate for their under-resolution or even omission in some cases of the sheet of vorticity that is shed into the flow immediately behind the blades.

The two-dimensional aerodynamic characteristics of the rotor blade sections are specified in a look-up table as a function of angle of attack and Mach number for a given Reynolds number. These characteristics can be used to precondition the zero through-flow boundary condition to allow the blade aerodynamic calculation to match closely the sectional aerodynamic characteristics, including stall, of the actual blade. As this approach is still essentially inviscid, the profile drag of the blade is calculated as a separate function of local angle of attack and is then added to the local aerodynamic force that is calculated from the blade aerodynamic model.

2.2.3 Fuselage Model

Fuselages or other solid bodies are represented using an unsteady vortex panel method, as described in Ref. 16. The surface of any body immersed in the flow field is discretised into a system of panels, such that each panel edge is represented as a vortex filament with constant strength, forming a closed loop of vorticity. The velocity at the centroid of any panel is calculated as the sum of the influences from all vortex filaments on the body together with the velocity induced by all the other vorticity within the flow. To determine the strengths of the vortex loops, a boundary condition of zero throughflow is enforced simultaneously at the centroids of all panels. Where present in the simulations described in this paper, the drive housing for the HART II rotor was modelled using 1908 panels. This yields a level of resolution that is comparable to previous simulations using this approach, for example as described in Ref. 16.

2.2.4 Structural Dynamics

In the particular version of the model that was used in the present investigation, the motion of the blades is prescribed, based on a variable-separable interpolation of the blade deformations that were measured at discrete azimuthal and radial locations on each blade during the HART II experiment. The blade deformation was measured using a non-intrusive optical method, called Stereo Pattern Recognition, as described in Refs. 17–19.

Each component D of the blade deformation is reconstructed in the simulations by using interpolating functions of the form

$$D(r,\psi) = \sum_{i=1}^{N_r} \sum_{j=1}^{N_a} a_{ij} P_i(r) F_j(\psi), \tag{10}$$

where N_r and N_a are respectively the number of radial and azimuthal interpolation functions $P_i(r)$ and $F_j(\psi)$ used to describe the particular component of the blade deflection. The radial interpolation functions were taken to be polynomials and the azimuthal interpolation functions were taken to be the components of a Fourier series so that

$$P_i(r) = r^{(i-1)} \tag{11}$$

and

$$F_j(\psi) = \begin{array}{cc} \cos\frac{j-1}{2}\psi & \text{if} \quad j \in \{1,3,5,\ldots\} \\ \sin\frac{j}{2}\psi & \text{if} \quad j \in \{2,4,6,\ldots\}. \end{array} \tag{12}$$

The coefficients a_{ij} of the interpolation function were calculated by enforcing a simple least squares fit to the measured data for the blade deformations. This method interpolates over the relatively sparse experimental data as well as fills any gaps in the data where the markers used in the measurements could not be viewed because they lay within the shadow of the drive enclosure and the mounting support, or had peeled off the blades. Throughout, the structural dynamics of the blades were prescribed using six interpolation functions in the radial direction and nine in the azimuthal direction. The sets of coefficients that give the best approximation to the elastic flap, lag and torsional deformations z_{el}, y_{el} and θ_{el} of the blades when using a basis with these dimensions are given in Ref. 9 for the HART II baseline, minimum vibration and minimum noise test cases.

The difference between the interpolation and the experimental data set for each of the measured components of the elastic deformation of the blades was within the stated error bounds on the measurements of $\pm 0.5^\circ$ for the elastic torsion and ± 0.5mm for the flap and lag deflections. Nevertheless, the reliability of the interpolation may be questioned in areas where the experimental data was particularly sparse, as was for instance the case around 0° and 180° azimuth.

2.3 Acoustic Analysis

The acoustic field that is radiated by the rotor is computed using a post-processor for the blade aerodynamic loads that implements the Farassat-1A formulation of the Ffowcs Williams-Hawking equations [20]. This formulation is widely used in rotor acoustic calculations because of the efficiency and accuracy that results from its analytic representation of the observer time derivatives. The aerodynamic force contributed by each blade panel is used to construct a point acoustic source at the centre of each panel. The loading noise at any given observer location is then obtained by summation of these acoustic sources. The aerodynamic model assumes an infinitesimally thin blade; the thickness noise has thus to be modelled independently. This is done by attaching a source-sink pair to each blade panel. Noise due to quadrupole terms is neglected in the present work. The method that was used to calculate the acoustic field did not account for absorption and scattering due to the presence of the drive enclosure even when it was included in the aerodynamic calculation.

3 AIRLOAD PREDICTIONS

The results of VTM calculations are compared for the three flight cases of the HART II test – the BL case with conventional control inputs, and the two cases with higher harmonic control inputs applied to the rotor – the so-called MV and MN cases. In addition, simulations of the HART II BL case at three different spatial and temporal resolutions (as summarised in Table 2) and simulations of the MN and MV cases at two of the three different resolutions were compared to expose the effect of grid resolution on the ability

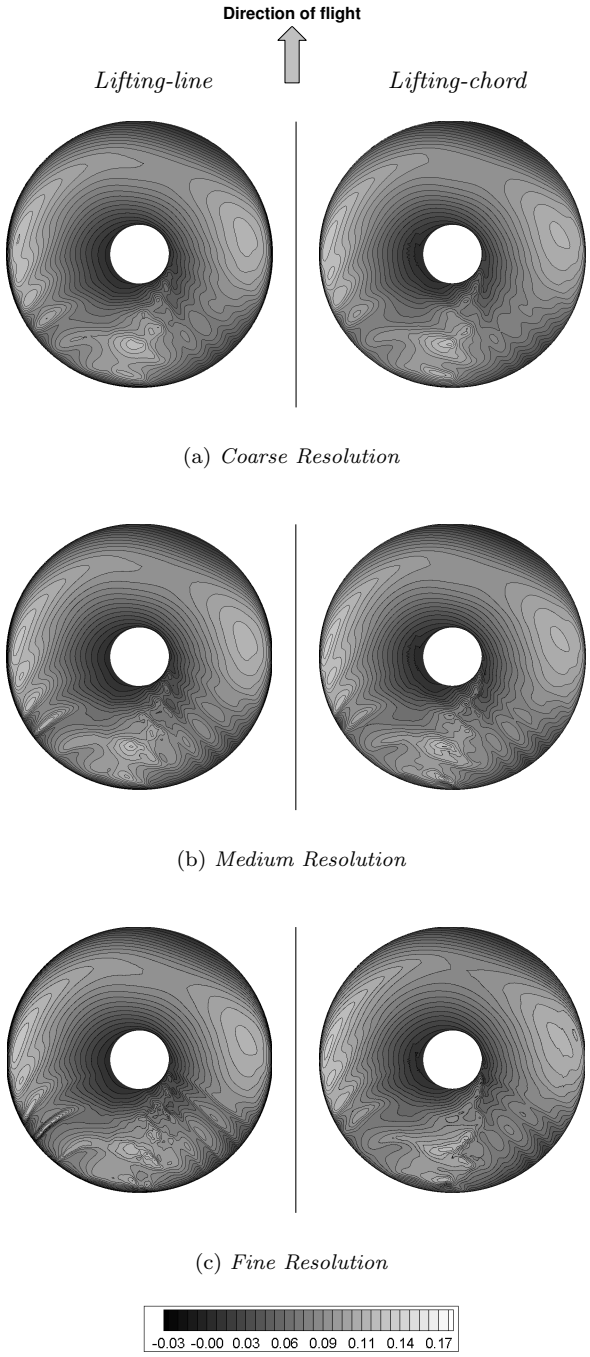

(a) *Coarse Resolution*

(b) *Medium Resolution*

(c) *Fine Resolution*

Figure 1: *Contours of non-dimensional lift ($C_N M^2$) as predicted by the VTM at various computational resolutions using the lifting-line and the lifting-chord representations of the blade aerodynamics.(HART II BL case)*

of each of the blade models described earlier to predict the airloads on the rotor. In all cases, the rotor was trimmed to the experimental thrust coefficient and to zero aerodynamic pitch and roll moments about its hub.

Table 2: Computational Resolution

	size of smallest cells		timesteps per rotor revolution	degrees per timestep
coarse	R/55.5	c/3.36	350	1.03°
medium	R/83.3	c/5.04	525	0.69°
fine	R/125.0	c/7.56	800	0.45°

3.1 Predictions of the overall blade airload

Figure 1 shows the predicted non-dimensionalised normal force coefficient ($C_N M^2$) for the HART II BL case, plotted as a series of contours over the rotor disc. The airload predicted by the VTM at each of the three different resolutions of the flow field defined in Table 2, and using the lifting-line and lifting-chord models for the blades are compared. The blade vortex interactions are visible in the contour maps as thin ridges of relatively high loading towards the rear of the disc, in the first and fourth quadrants of the rotor. The interactions are strongest outboard towards the blade tips, particularly on the retreating side of the disc. Where the lifting-line approach is used, an increase in grid resolution results in a marked increase in the amplitude of the BVI peaks and the associated loading gradients become significantly steeper. In contrast, the lifting-chord approach shows much less sensitivity to the size of the computational cells.

During the HART II test programme, the sectional airload, C_N, at 87% of the blade span was estimated by conditionally averaging the signal from a set of pressure transducers mounted at this section of the blade. Figure 2 compares the measured blade airload at this radial station for the three HART II flight cases, expressed in terms of non-dimensionalised normal force coefficient ($C_N M^2$), to the loading predicted by the VTM. In general, the calculated loading on the rotor compares well with the experimental data for all flight cases.

The advancing side is perhaps the least well resolved, with the largest discrepancies between prediction and experiment on this side of the disc occurring in the low-frequency component of the airload. The discrepancies in this component of the airload are similar regardless of computational resolution and also irrespective of the model that is used to represent the aerodynamics of the blade. As it is this component of the loading that is primarily affected by control inputs and blade structural deformation, it is most likely that these discrepancies are due to errors in the interpolation that was used to prescribe the blade dynamics within the simulation, as discussed in Refs. 9–11.

The predictions of the loading on the retreating side

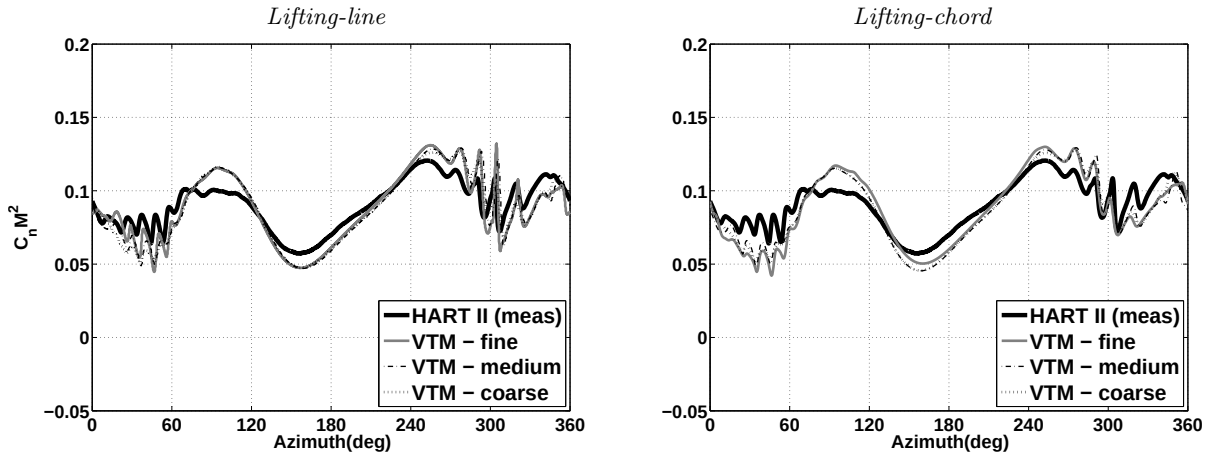

(a) *Baseline case*

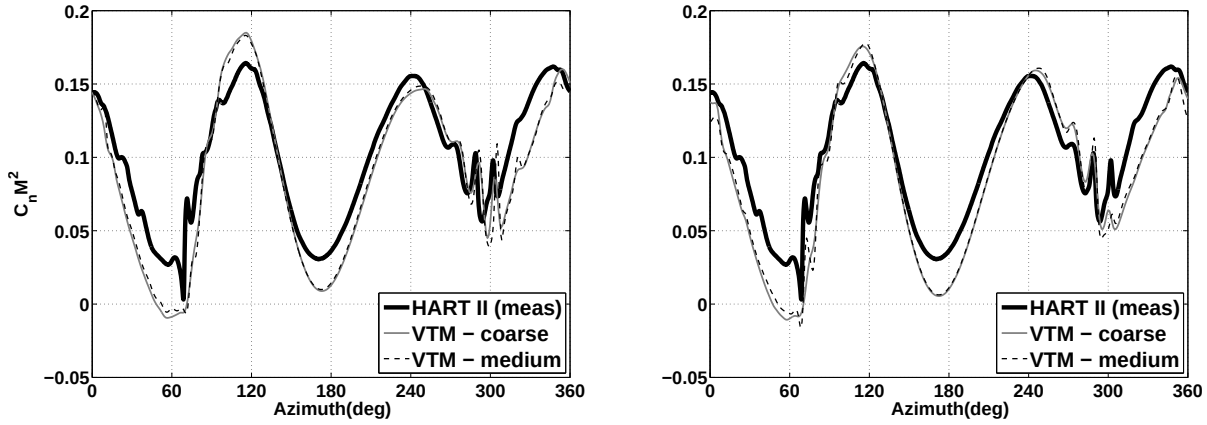

(b) *Minimum Noise case*

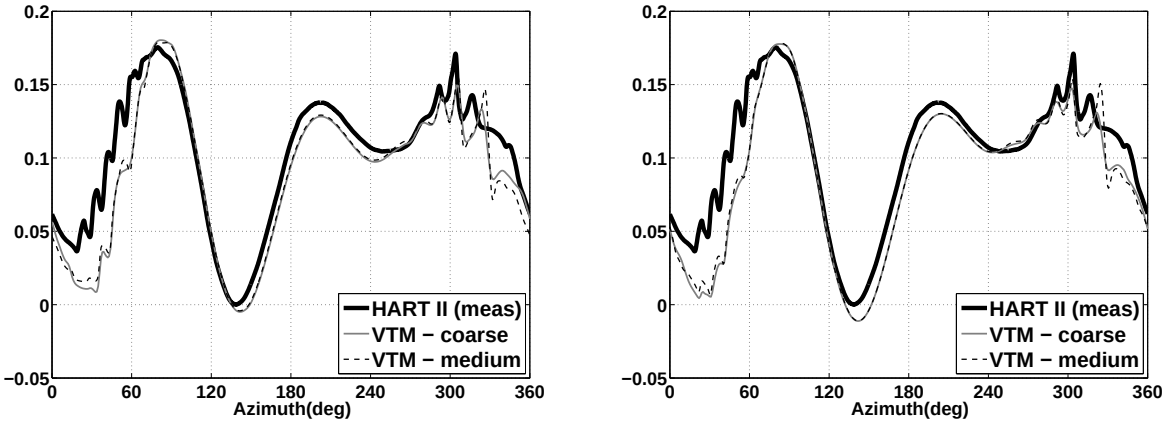

(c) *Minimum Vibration case*

Figure 2: *Comparison of blade loading ($C_N M^2$) at 87% span, as predicted using lifting-line and lifting-chord representations of the blade aerodynamics, against experimental data for all three HART II flight cases*

of the disc correlate well with the experimental data for all three flight cases. The figures show nevertheless that the lifting-line method is more sensitive to changes in the cell size used to represent the wake than the lifting-chord approach. Indeed, the differences between the predictions of the two models are most obvious in their representation of the high-frequency components of the blade airload.

3.2 Predictions of the high-frequency component of the blade airload

The high-frequency component of the blade airload is almost exclusively due to the localised interactions between the rotor blades and the vortices within the rotor wake. In Fig. 3 the contours of the predicted non-dimensionalised normal force coefficient ($C_N M^2$) have been filtered to include only the high frequency components of the signal, i.e. those greater than ten per rotor revolution, to expose in greater detail the distribution of BVI events across the rotor disc.

This figure shows clearly the effect of HHC inputs on the position and strength of the BVIs. In the BL case, in which no higher harmonic control is applied, the BVI loading peaks are located outboard on the rotor disc and towards its rear, i.e. in quadrants one and four. The interactions on the retreating side of the disc are stronger as the interacting vortices are orientated more nearly parallel to the blade than on the advancing side.

In comparison to the BL case the BVI events in the MN case, particularly within the first quadrant on the advancing side of the rotor, are located significantly more inboard. Moreover, the tip vortices pass close to the disc further forward than in the BL case, and thus the area of the disc over which the BVI events occur extends more forward. Since the Mach number of the blade increases towards the tip, those interactions which occur inboard take place at lower Mach number. On the retreating side, again the positions of the BVIs are more forward in the MN case than in the BL case, and, as a result, the interacting vortices are no longer orientated parallel to the blade. Both these effects act together to reduce the amount of noise that is radiated towards the ground.

In the MV case the azimuthal locations of the BVI events remain similar to those of the BL case on both the advancing and retreating sides of the rotor but the associated loading peaks are shifted more outboard towards the blade tips. The higher Mach numbers associated with these interactions produce an increase in the noise radiation from both sides of the disc. These trends are comparable to those obtained by plotting the experimentally measured pressure along the leading edge of the blade for the three HART II flight cases [1, 2]. The computations also reveal the presence of relatively strong interactions with the root-vortex system that is produced by the blades. These interactions are not apparent in the experimental data, however, and may be an artifact of the omission of any representation of the rotor hub assembly from the calculations.

Figures 4-6 show the non-dimensionalised normal force coefficient ($C_N M^2$) for the measured radial station at 87% span, after it has been filtered to contain only the high-frequency component of the loading. In

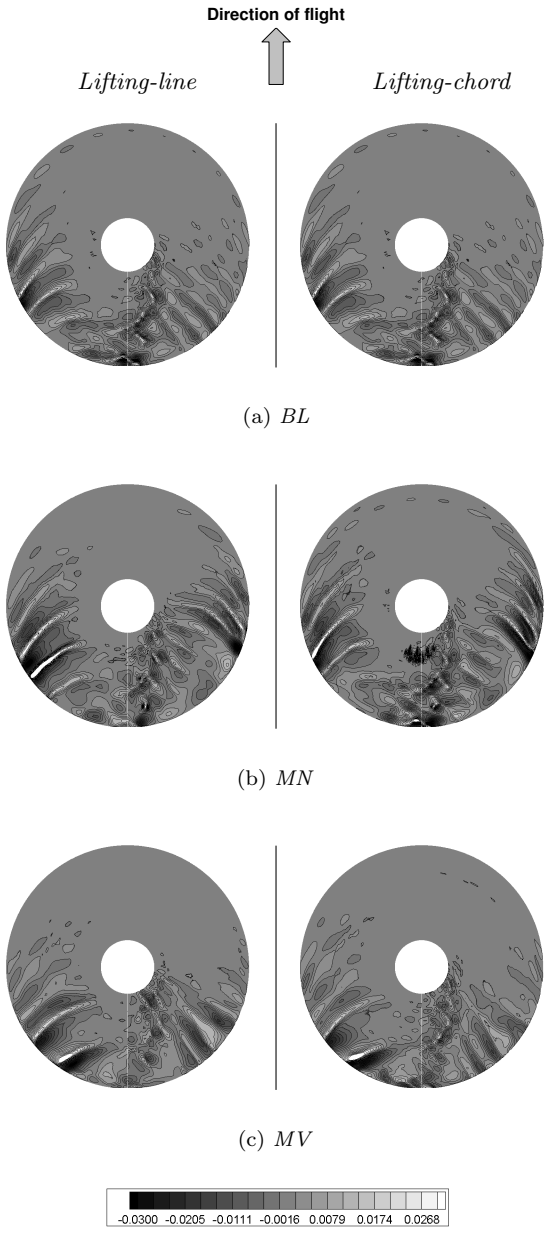

Figure 3: *Contours of non-dimensional lift ($C_N M^2$) as predicted by the VTM at the medium computational resolution using the lifting-line and the lifting-chord representations of the blade aerodynamics. The signal has been filtered to include only the higher harmonic components, greater than 10/rev.*

these figures, the BVI-induced loading fields on the retreating and advancing sides of the rotor have been produced with expanded azimuthal scale to aid their interpretation.

For each of the flight cases, the numerical representation of the BVI events on the retreating side of the rotor is generally satisfactory, apart from a rather gross mis-representation of the amplitude and position of the furthest-aft BVI in the MV case. In addition, the predicted amplitude of this loading peak is very sensitive to the cell size used in the simulation. Indeed, the differences in the grid-sensitivity of the two blade aerodynamic models in their prediction of the BVI-induced loading are most obvious on this side of the disc. A marked improvement in the accuracy of the predicted high-frequency airloads of the HART II rotor is obtained when the lifting-chord model for the blade aerodynamics is used instead of the lifting-line type approach. Errors in the amplitude and phase of the BVI-loading peaks are generally reduced and the quality of the prediction is affected to a lesser extent by the computational resolution.

In Ref. 11 it was argued that the deficiencies in prediction of the BVI-induced airloads when the lifting-line model is used are due to a mis-representation of the aerodynamic response of the blade when subjected to the very localised perturbations in its aerodynamic environment that are characteristic of helicopter blade vortex interactions. With its single-point boundary condition, the lifting-line model is overly sensitive to the maxima and minima within the velocity field that is encountered by the blade. The lifting-chord model is less sensitive to the localised, small-scale features of the flow field and its predictions are dependent more directly on the integral, invariant properties of the flow field such as the circulation of the individual tip vortices.

For all three flight cases, all the BVIs on the advancing side of the rotor are captured by the numerics, but there are errors in the phasing and amplitude of the BVI-induced loading peaks in almost all cases. The MN and MV cases (Figs. 5 and 6 respectively) show somewhat greater discrepancy between the predictions and the experimental data than the BL case.

In the BL case there is generally good agreement between measurement and prediction, but the strongest BVI event on the advancing side of the disc is slightly mis-represented by the numerical method. In the measured signal the loading peak with the largest amplitude occurs at approximately 50° azimuth. In contrast, the numerical calculations using both medium and fine grid resolutions predict the BVI event that occurs at an azimuth of 40° to be marginally stronger than the BVI at 50°. The predicted loading intensity is thus shifted towards the rear of the disc compared to experiment. At the finest computational resolution, the difference in magnitude between each of these two BVI impulses is minimal, however. It is believed that this sensitivity in the relative strength of these BVIs to the computational resolution has a strong influence on the predicted position of the acoustic maximum on the advancing side of the disc, as will be described in the next section of this paper.

In the MN case, the most intense BVI impulse, at an azimuth of 70° on the advancing side, is under-predicted in amplitude when the lifting-line model is used, regardless of the resolution of the flow-field. In contrast, as the grid resolution is increased the lifting-chord model very accurately captures this particular loading peak.

Figure 7 compares the wake structure that is predicted by the VTM at the medium resolution for the MN case when the lifting-chord representation of the aerodynamics of the blade is used to that predicted when the lifting-line model is used. This figure shows the sensitivity of the predicted wake structure to the model that is used to represent the blade aerodynamics. In the calculation in which the lifting-line model has been used, the vortex that is responsible for the most prominent BVI in the MN case passes beneath the blade whereas when the lifting-chord model is used the vortex passes above the blade. It has been shown previously that the VTM predicted airloads are sensitive to the very subtle changes in the vorticity distribution which is sourced into the flow by the blades when different blade aerodynamic models are used, and in this case, given the shallow angle between the vortex and the blade, it can easily be conceived how a small change in the predicted position of the vortex could have a large effect on the predictions of the associated BVI airload.

4 ACOUSTICS

4.1 Sound Pressure Levels

The accuracy of the airload predictions, particularly of the loads that are induced by blade vortex interactions, influences directly the accuracy to which the acoustic signature of the rotor can be predicted. In the HART II experiment, noise measurements were performed with an array of 13 microphones mounted transversally to the axis of the tunnel on a ground plane that was located 2.215m (1.1R) below the rotor hub. A map of the sound intensity on the ground plane was generated by moving this microphone array along the axis of the tunnel. Figures 8-10 compare the measured sound pressure level (SPL) to that computed from the airloads which were predicted by the VTM. In all cases the data has been filtered to include only the frequencies between 6-40 times the blade passage frequency. This is generally accepted to be the range that is dominated by BVI noise.

The acoustic calculation does not account for the

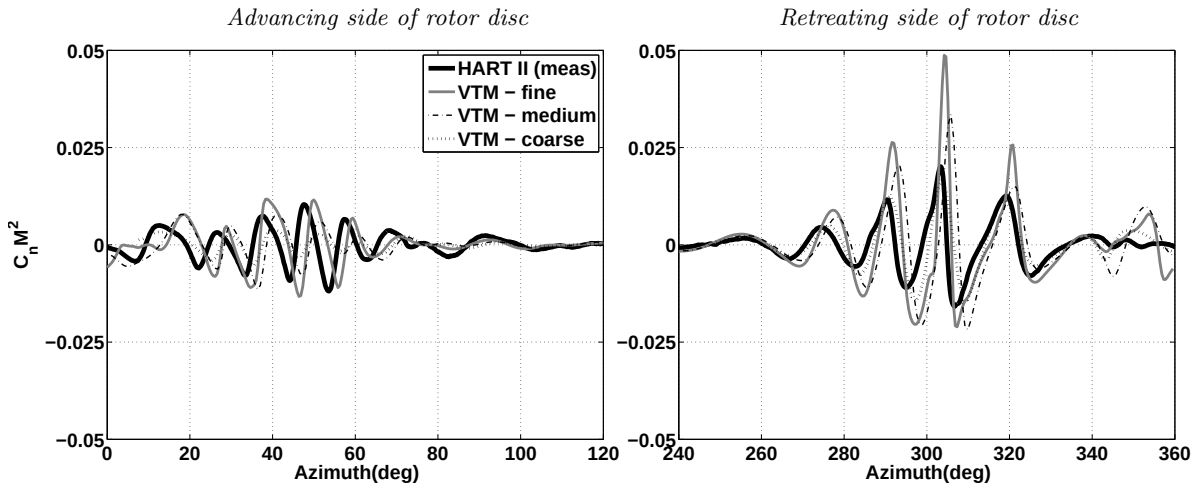

(a) *Lifting-line model*

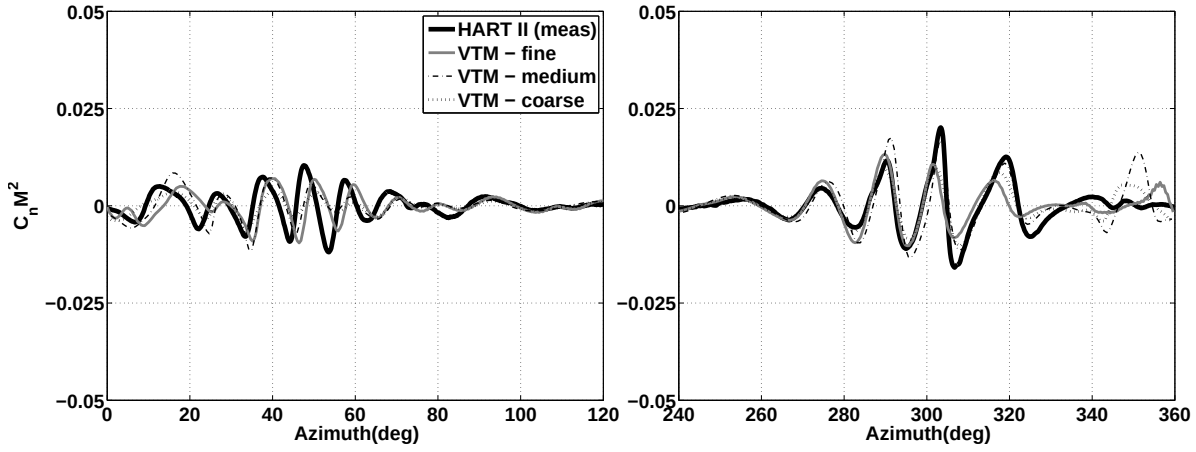

(b) *Lifting-chord model*

Figure 4: *Comparison of blade loading (C_NM^2) at 87% span, as predicted using lifting-line and lifting-chord representations of the blade aerodynamics, against experimental data for the HART II BL case. The signal has been filtered to include only higher harmonic components (>10th harmonic).*

scattering and absorption of acoustic energy by solid bodies within the flow, and whilst this does not affect the principal sources of sound in the flow-field it does influence the distribution of noise once it reaches the ground plane. This deficiency is visible in Fig. 8 for the BL case, for example, where scattering and absorption by the drive enclosure (fuselage) is responsible for the thin region of reduced noise that is present in the experimental data (Fig. 8(a)) in the centre and to the rear of the rotor disc but which is not captured by the numerical method (Fig. 8(b-d)).

For all three of the HART II flight cases, the distribution of acoustic pressure on the ground plane is characterised by two acoustic maxima which occur one on the advancing side and one on the retreating side of the disc. The sound pressure can also be seen to decay rapidly upstream of the rotor towards the retreating side of the disc. The experimental results show the maximum SPL on the ground plane to be lower in the MN case than in the BL case and the directivity to be shifted towards the front of the rotor. In contrast, the maximum SPL in the MV case is higher but the directivity pattern is similar to that in the BL case.

In general, as is the case with the airload predictions, the SPL predicted by the VTM shows a better correlation with the measured data on the retreating side of the disc than on the advancing side. The upstream decay in the noise level on the retreating side of the rotor disc, which is present in both the BL and MV cases, is well resolved irrespective of the aerodynamic model or the computational resolution that is used. The directivity of the sound is therefore cap-

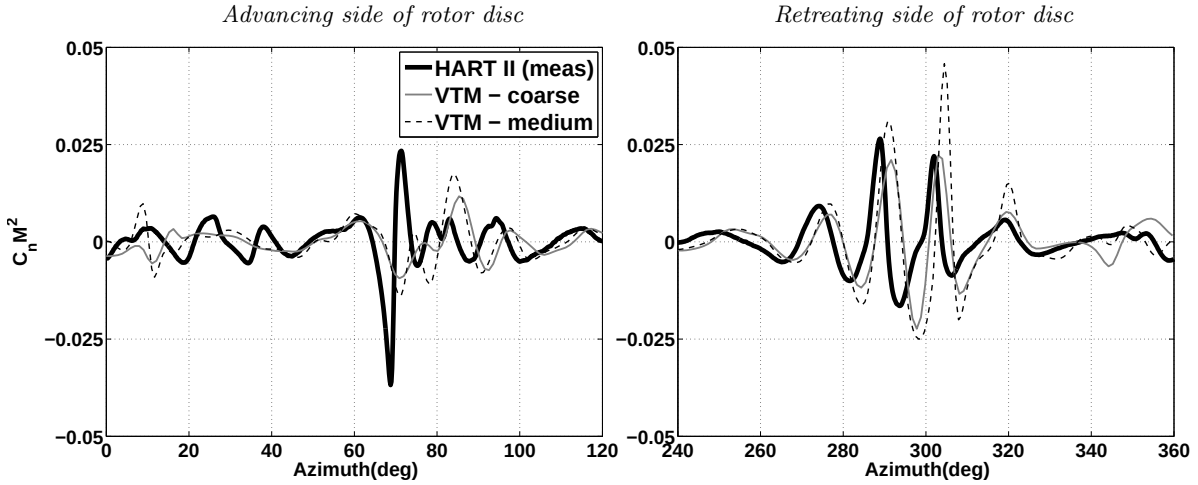

(a) *Lifting-line model*

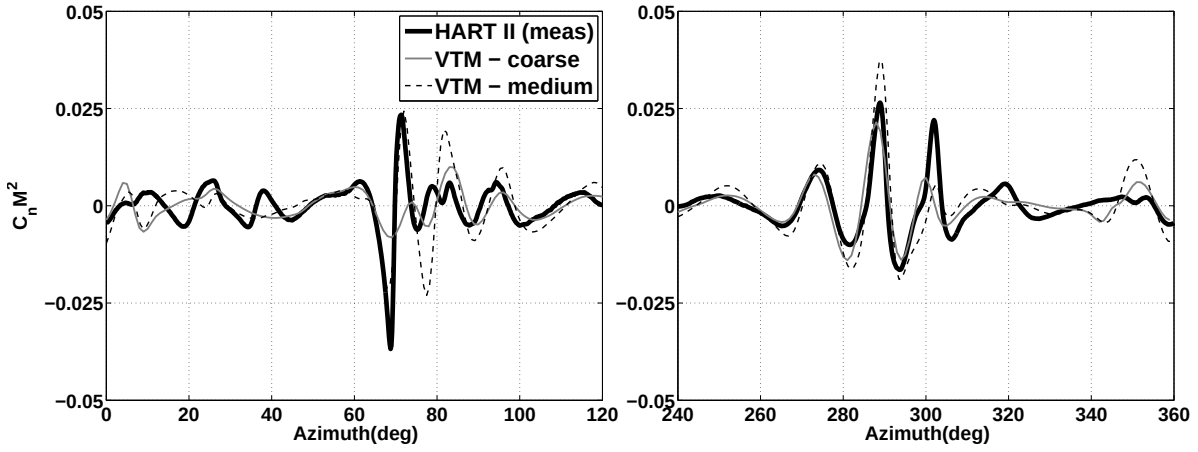

(b) *Lifting-chord model*

Figure 5: *Comparison of blade loading (C_NM^2) at 87% span, as predicted using lifting-line and lifting-chord representations of the blade aerodynamics, against experimental data for the HART II MN case. The signal has been filtered to include only higher harmonic components (>10th harmonic).*

tured well by the numerical method. The change in directivity found in the MN case compared to the BL case is also captured reasonably well by the numerics. The two SPL maxima, present in all the test cases, are also captured in the numerical predictions, albeit with some errors in their position and peak SPL value. The SPL maximum on the retreating side of the disc is generally more accurately captured, both in terms of its position and its amplitude, than the maximum that is present on the advancing side of the disc.

Where the lifting-line approach is used to model the aerodynamics of the blades, the over-prediction in the amplitude of the BVI loading peaks with increase in the grid resolution translates into an over-prediction of the acoustic pressure levels on the ground plane beneath the rotor. Indeed, the peak value of the SPL at the maxima on both sides of the rotor increases significantly as the computational resolution is increased. The lifting-chord approach shows much less sensitivity to the computational resolution of the wake, with the result that the predicted peak value of the SPL, particularly at the maximum on the retreating side of the disc, compares well with the measured value. The method does still however over-predict the maximum noise levels when the finest computational resolution is used, although to a much lesser extent than when the lifting-line approach is adopted.

The reason for this behaviour is relatively straightforward. As the resolution of the computation is increased, the convection algorithm used within the VTM acts to resolve the vortex core over a smaller and smaller area, with the result that the vortical structures

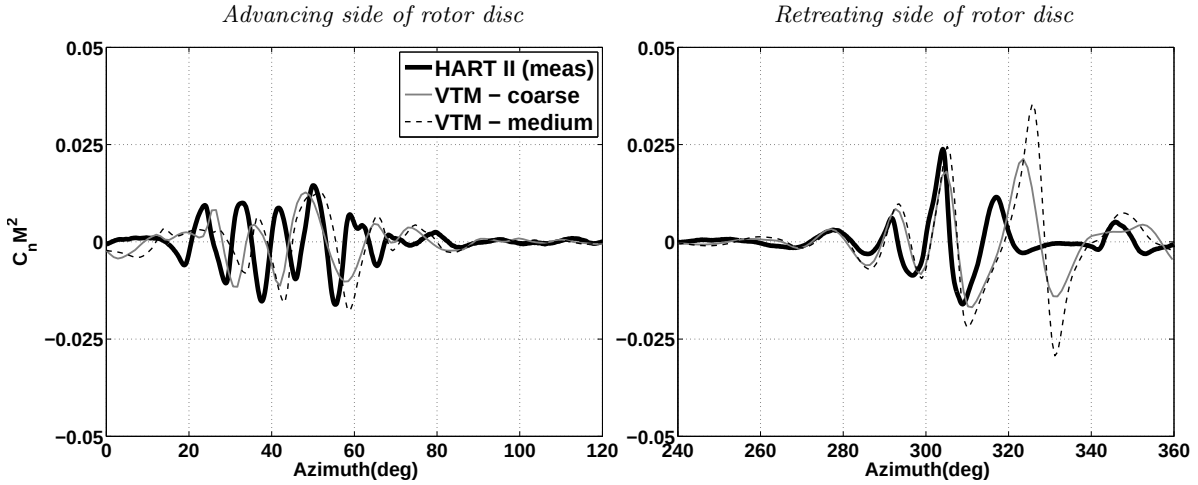

(a) *Lifting-line model*

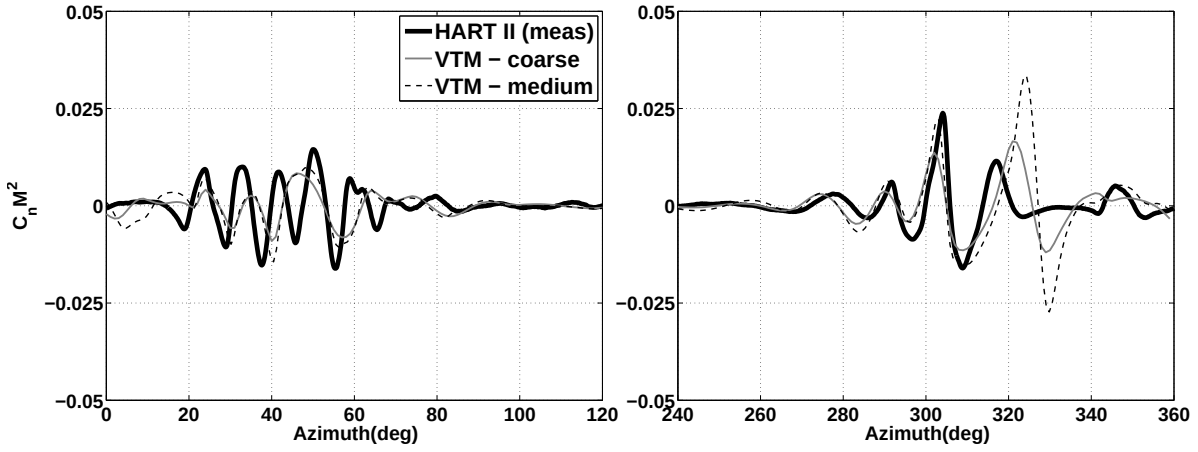

(b) *Lifting-chord model*

Figure 6: *Comparison of blade loading ($C_N M^2$) at 87% span, as predicted using lifting-line and lifting-chord representations of the blade aerodynamics, against experimental data for the HART II MV case. The signal has been filtered to include only higher harmonic components (>10th harmonic).*

become more and more concentrated. A smaller vortex core radius for a given vortex strength implies higher peak velocities in the vortex. These produce more impulsive changes in the loading and thus higher noise intensity when the vortex passes close to the blade. The VTM is known to preserve very accurately the circulation in the flow field [10] but as this circulation is is confined to fewer cells it results in an overly impulsive acoustic pressure when the vortex interacts with the blade. While the blade airload is less sensitive to maxima and minima in the velocity profile when using the lifting-chord approach, the acoustic post-processing method, depending as it does on the loading gradients rather than directly on the amplitude of the BVI-loading peaks, appears not to be so benign.

The calculations at both coarse and medium resolution predict the location of the SPL maximum on the advancing side of the rotor for all three HART II flight cases, except perhaps the MV case, to be further to the rear of the rotor disc than the position of the experimentally measured maximum. This discrepancy is marginally more apparent when the lifting-chord model is used than when the lifting-line model is used, even though the airloads are generally better predicted using the lifting-chord approach.

4.2 Acoustic Sources

It is instructive to examine the relationship between the noise produced at the acoustic maxima and the source of the noise in the individual BVI events on the

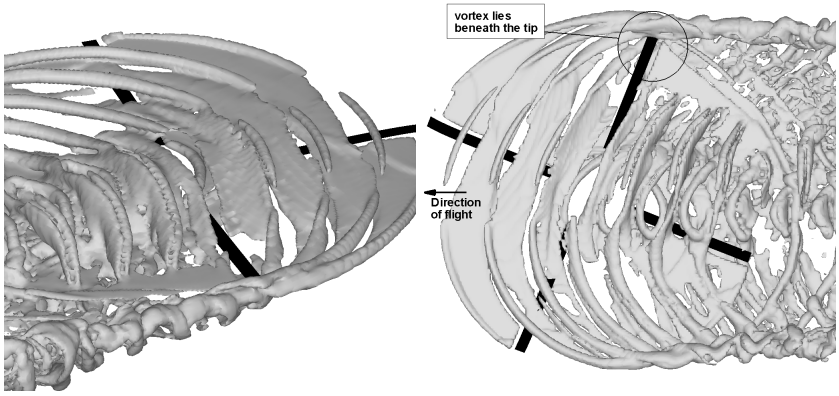

(a) *Lifting-line model*

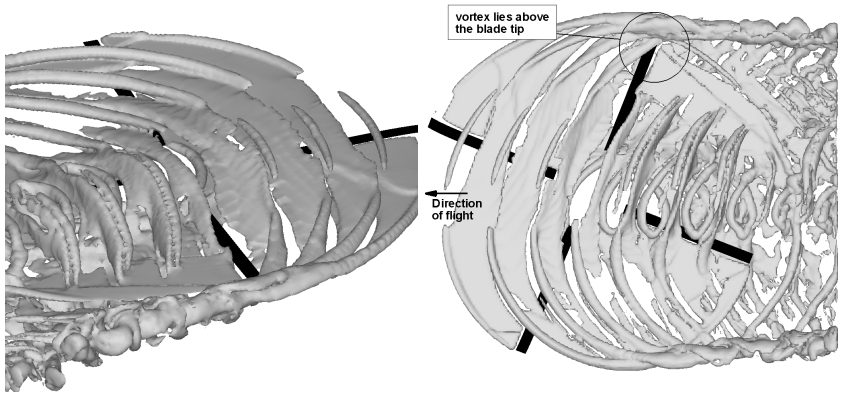

(b) *Lifting-chord model*

Figure 7: *Geometry of the BVI at 70° azimuth, as predicted using lifting-line and lifting-chord representations of the blade aerodynamics, for the HART II MN flight case.*

rotor. Parts (a) of Figs. 11–16 compare the predicted and measured time histories of acoustic pressure at the positions of the two microphones located at the points of measured maximum noise level on the advancing and retreating sides of the rotor for the BL case (Microphones M11 and M4 respectively). The positions of these microphones are represented by the small circles on the acoustic SPL plot in parts (b) of the same figures. The time histories are produced with expanded timescale corresponding to a single blade passage. The predicted distribution of acoustic source density due to loading on the disc is also plotted (in parts (b) of the figures) from the perspective of an observer located at the relevant microphone. The source density is evaluated from the loading noise term in the Ffowcs Williams-Hawking equations and is plotted in 'source time' – in other words the sources are located at their position on the disc when the sound at the particular observer time was generated. In parts (b) of Figs. 11–16, the white lines indicate the locus of sources at the time of several of the stronger acoustic features in the numerical predictions of the noise produced by the rotor. These loci can be used to identify the positions of the BVI events that are responsible for the corresponding acoustic feature – as is done in parts (c) of the figures.

In general the computations reproduce the BVI acoustic signature at the microphone on the retreating side of the rotor with the correct phase, but the amplitude of several of the acoustic peaks is very sensitive to the grid resolution and to the aerodynamic model that is used to represent the blade airloads. The lifting-chord model more accurately captures the phase of the signal and the accuracy of the prediction is influenced to a lesser extend by reducing the cell size than is the case when the lifting-line model is used. The measured acoustic signature at this microphone contains a group of three peaks which occur at observer times of 0.011s, 0.0128s and 0.0138s respectively. The corresponding numerically-predicted acoustic features are marked as

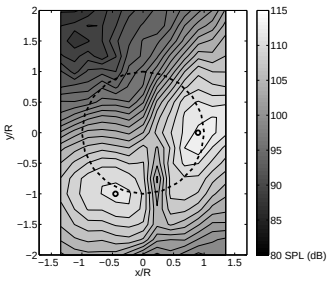

(a) *HART II measured*

Lifting-line *Lifting-chord*

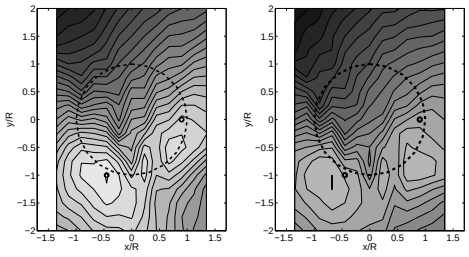

(b) *Coarse resolution*

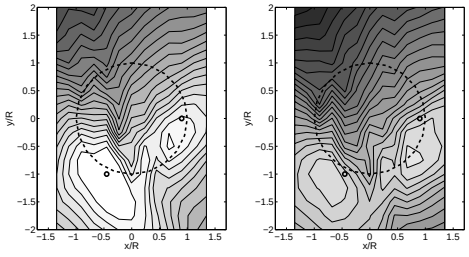

(c) *Medium resolution*

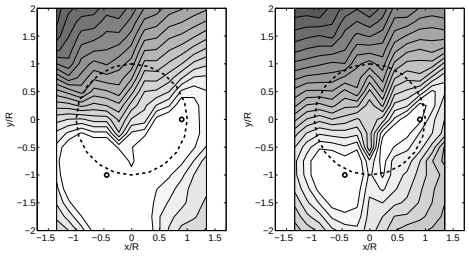

(d) *Fine resolution*

Figure 8: *Predicted and measured SPL noise contours for the HART BL flight case. (The rotor position is marked by a dashed circle).*

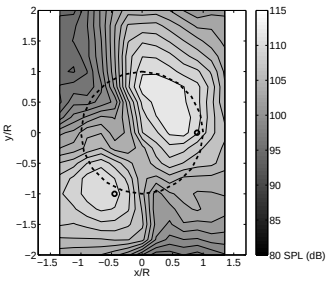

(a) *HART II measured*

Lifting-line *Lifting-chord*

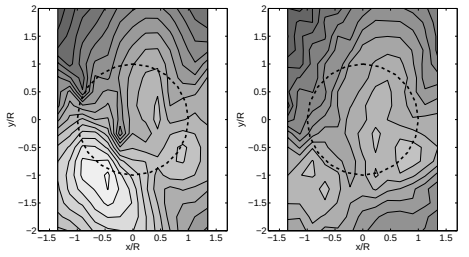

(b) *Coarse resolution*

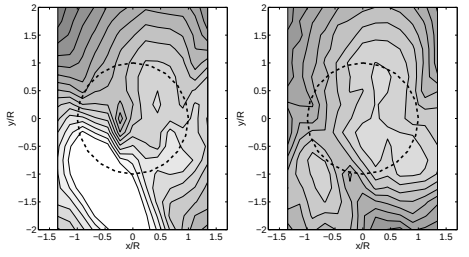

(c) *Medium resolution*

Figure 9: *Predicted and measured SPL noise contours for the HART MN flight case. (The rotor position is marked by a dashed circle).*

'A' and 'B' in Figs. 11–13 parts (a) and (b). The most intense feature – marked 'A' in Figs. 11–13 – is the result of the strong parallel BVI which occurs at a blade azimuth of about 300°. It is interesting to note that the lifting-chord model predicts this intense BVI to occur about 10° earlier than when the lifting-line model is used (Figs. 11–13 parts (c)). This shift may account for the consistent azimuthal discrepancy in the location of the SPL maximum on this side of the disc that is predicted by the two approaches. The reason for the rather obviously missing peak in the numerically-generated signal at an observer time of 0.011s has still to be determined, but the appearance (or not) of certain features in the acoustic signature is known to be

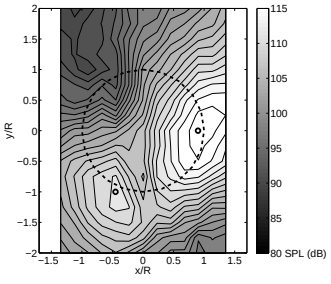

(a) *HART II measured*

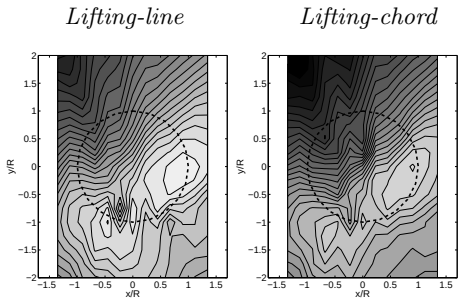

(b) *Coarse resolution*

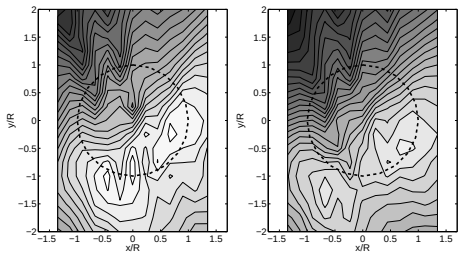

(c) *Medium resolution*

Figure 10: *Predicted and measured SPL noise contours for the HART MV flight case. (The rotor position is marked by a dashed circle).*

crucially dependent on occasion on the relative amplitude and phasing of several consecutive BVI events. The reason for this discrepancy may thus be difficult to localise.

The measured time history of acoustic pressure at the microphone located on the advancing side of the rotor disc is characterised by two strong acoustic pulses per blade passage (see parts (a) and (b) of Figs. 14–16), the stronger of which occurs at an observer time of approximately 0.0155s. The computations reproduce reasonably well the BVI noise signature at this location, but there is a consistent error in phase between the numerical and measured data. The amplitude of the predicted acoustic peaks is also very sensitive to the resolution of the flow-field no matter which blade model is used.

The principal peak in the predicted acoustic signature at the maximum on the advancing side of the rotor is associated with a BVI event on this side of the disc which occurs when the reference blade is located at approximately 40° azimuth (marked 'A' in Figs. 14–16). Figure 17 shows the geometry of the wake at this instant and reveals the root vortices which are extruded from blades 1, 2 and 3 as well as a relatively old tip vortex from blade 4 to be interacting strongly with the reference blade. As mentioned earlier, there is some question as to the accuracy of the representation of the root vortex system given the absence of any model of the rotor hub assembly in the simulations, and certainly any error in the prediction of the strength of the vorticity trailed from the roots of the blade would adversely affect the predictions of the flow and hence the acoustic pressure which is generated by the blades as they pass near the rear of the disc. An overly strong root vortex structure could quite feasibly distort the trajectories of the tip vortices that are responsible for the BVIs as they pass upward and through the zones of maximum BVI activity on the rotor disc, or indeed combine with the vorticity in the interacting vortex, resulting in an over-prediction of the intensity of the interaction. In all cases, the predominant peak in the acoustic signal at the maximum on the advancing side of the rotor occurs later in the simulations than in the experimental data, suggesting indeed that at least a small mis-placement of the vortex might be responsible for the discrepancies in the numerical representation of this acoustic feature.

5 CONCLUSIONS

Aerodynamic and acoustic predictions using Brown's Vorticity Transport Model (VTM) are compared against the HART II wind tunnel data for an experimental model based on the characteristics of the Bo105 rotor. The rotor was flown in a descending flight condition in which the loading on its blades contained significant high-frequency content due to the presence of blade vortex interactions. This data has been used in the present paper to analyse the ability of two blade aerodynamic models to capture the detailed, high frequency, BVI-induced loading on the rotor and thus the acoustic signature of the aircraft. The first model is an extension of the Weissinger-L lifting-line model, in which the strength of a bound vortex, placed at the quarter-chord of each blade panel, is determined by imposing a zero-through flow boundary condition at a single point located at the three-quarter chord of the panel. This approach is compared to a second, 'lifting-chord' method that is based on classical unsteady thin

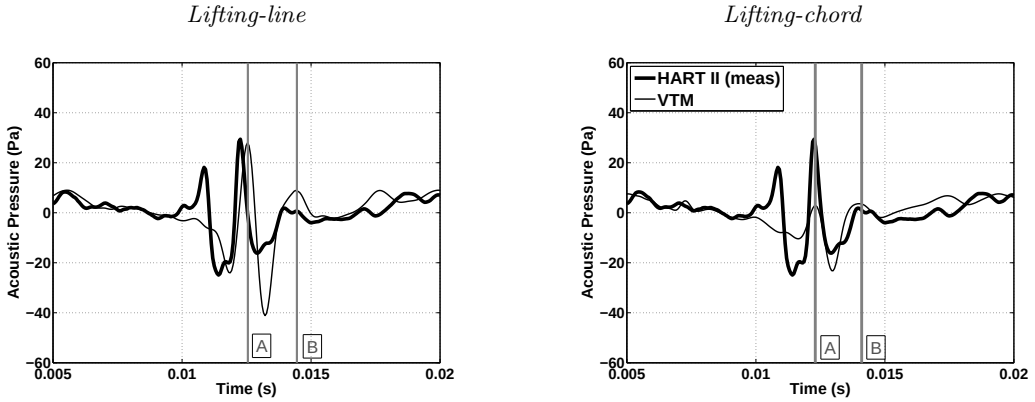

(a) *Time history of acoustic pressure for a single blade passage*

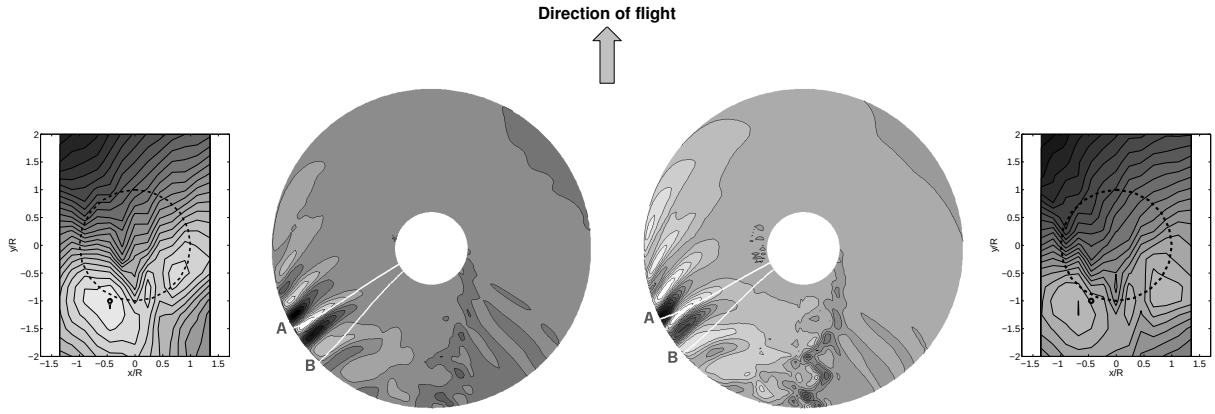

(b) *Predicted acoustic source density (loading noise, Pa/m^3)*

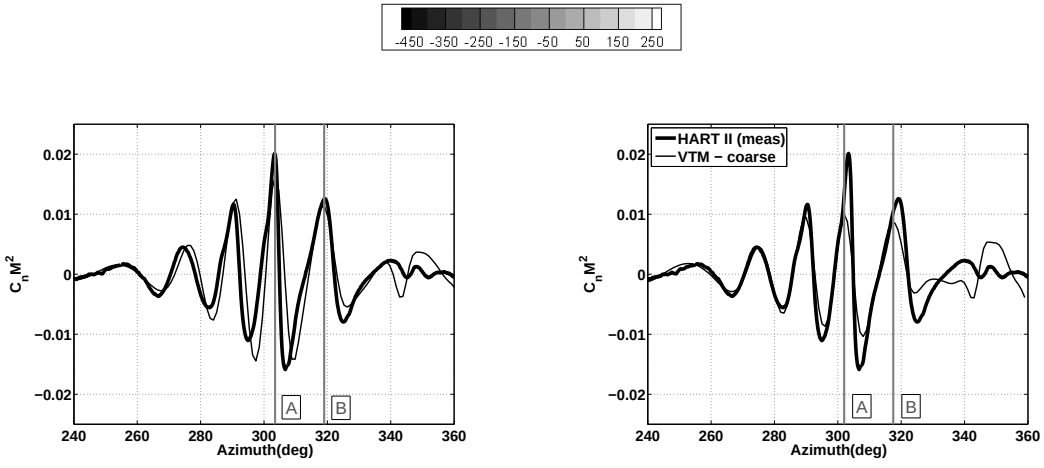

(c) *BVI-induced airloads*

Figure 11: *Time history of acoustic pressure for one blade passage and the corresponding BVI-induced airloads and source density distribution on the rotor for an observer located at the experimentally-measured SPL maximum on the retreating side of the rotor (HART II BL case). Numerical results are for the coarse computational resolution.*

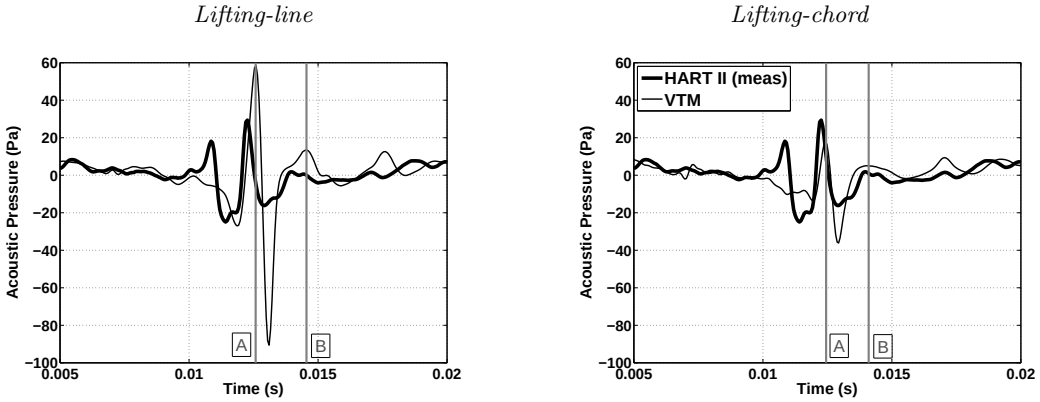

(a) *Time history of acoustic pressure for a single blade passage*

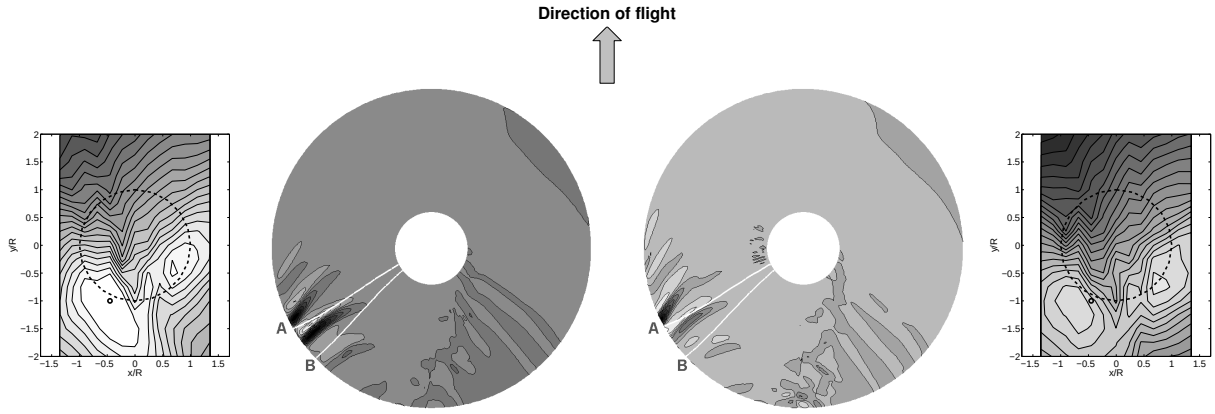

(b) *Predicted acoustic source density (loading noise, Pa/m^3)*

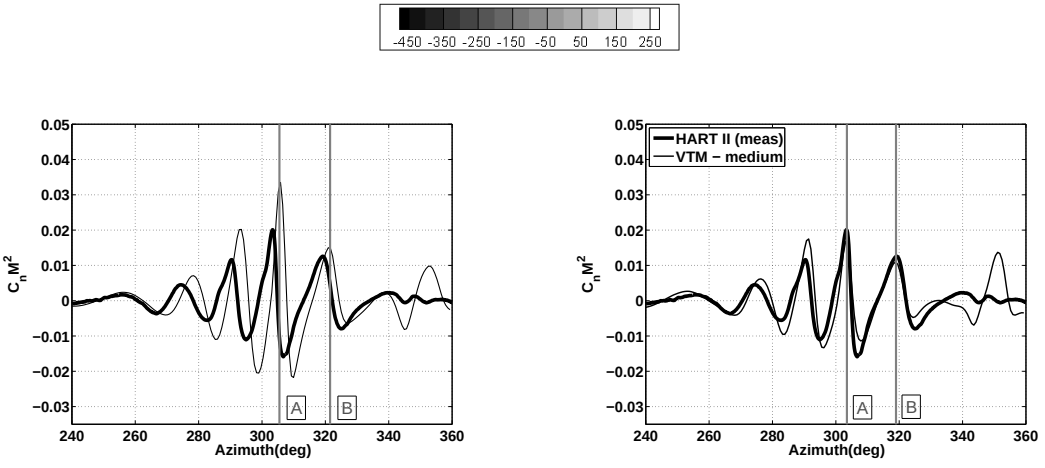

(c) *BVI-induced airloads*

Figure 12: *Time history of acoustic pressure for one blade passage and the corresponding BVI-induced airloads and source density distribution on the rotor for an observer located at the experimentally-measured SPL maximum on the retreating side of the rotor (HART II BL case). Numerical results are for the medium computational resolution.*

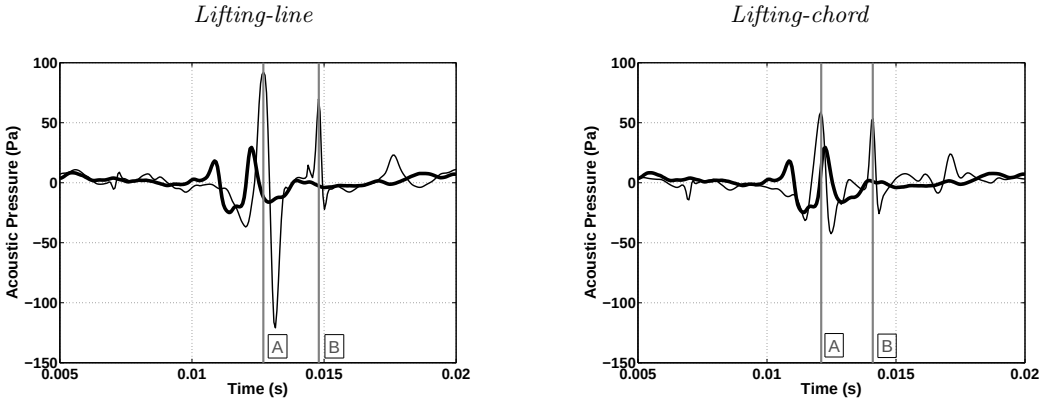

(a) *Time history of acoustic pressure for a single blade passage*

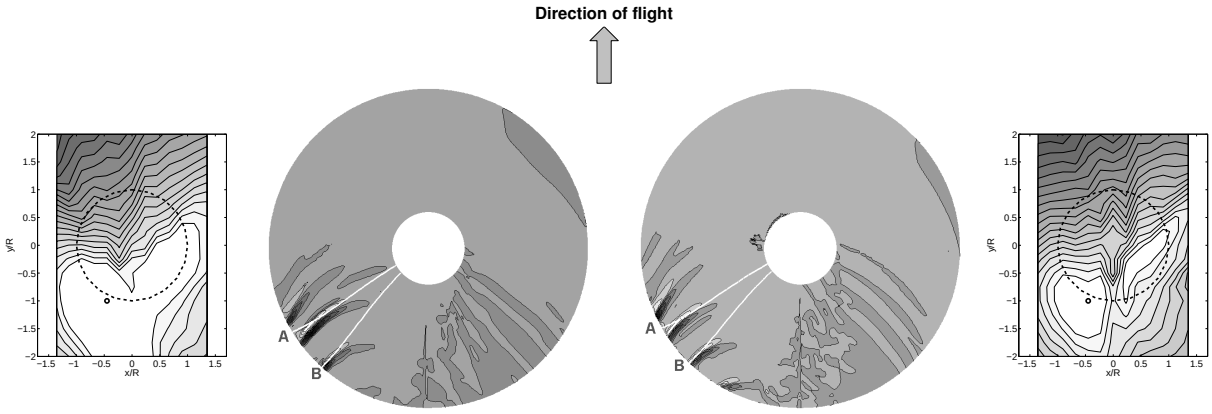

(b) *Predicted acoustic source density (loading noise, Pa/m^3)*

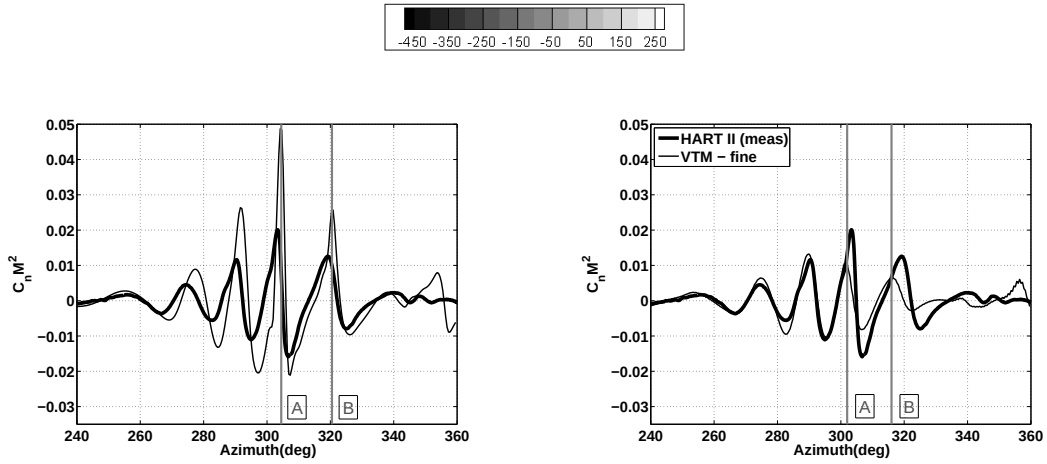

(c) *BVI-induced airloads*

Figure 13: *Time history of acoustic pressure for one blade passage and the corresponding BVI-induced airloads and source density distribution on the rotor for an observer located at the experimentally-measured SPL maximum on the retreating side of the rotor (HART II BL case). Numerical results are for the fine computational resolution.*

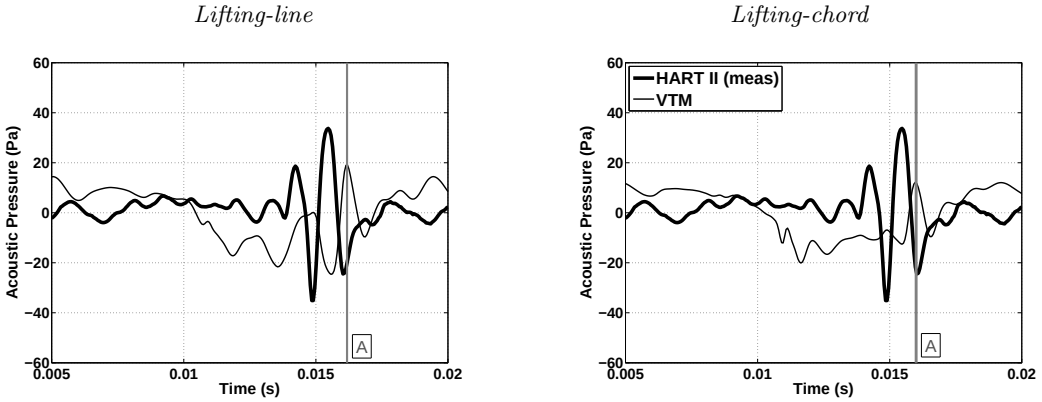

(a) *Time history of acoustic pressure for a single blade passage*

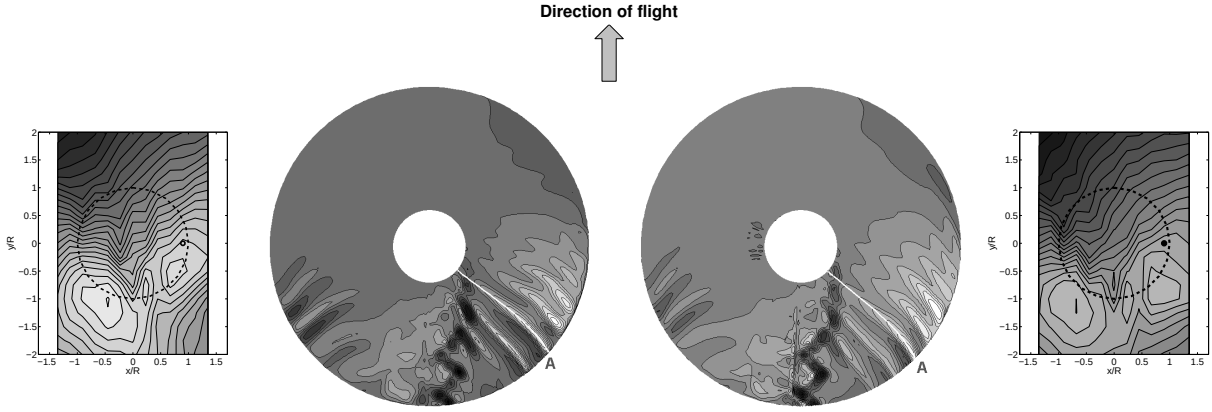

(b) *Predicted acoustic source density (loading noise, Pa/m^3)*

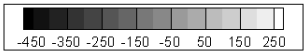

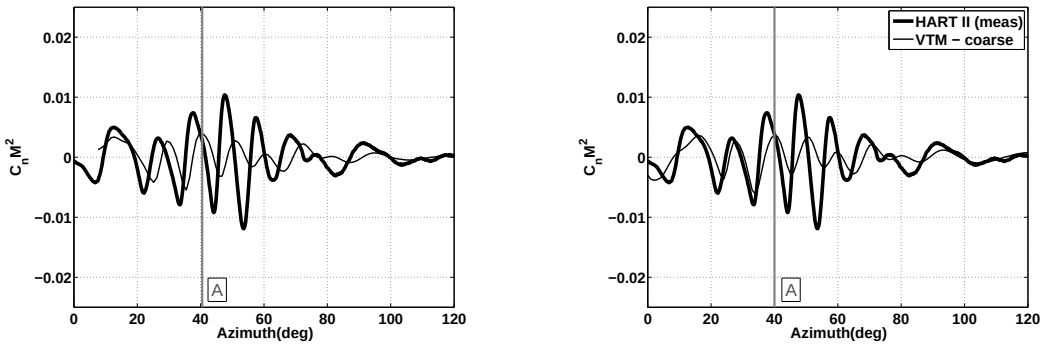

(c) *BVI-induced airloads*

Figure 14: *Time history of acoustic pressure for one blade passage and the corresponding BVI-induced airloads and source density distribution on the rotor for an observer located at the experimentally-measured SPL maximum on the advancing side of the rotor (HART II BL case). Numerical results are for the coarse computational resolution.*

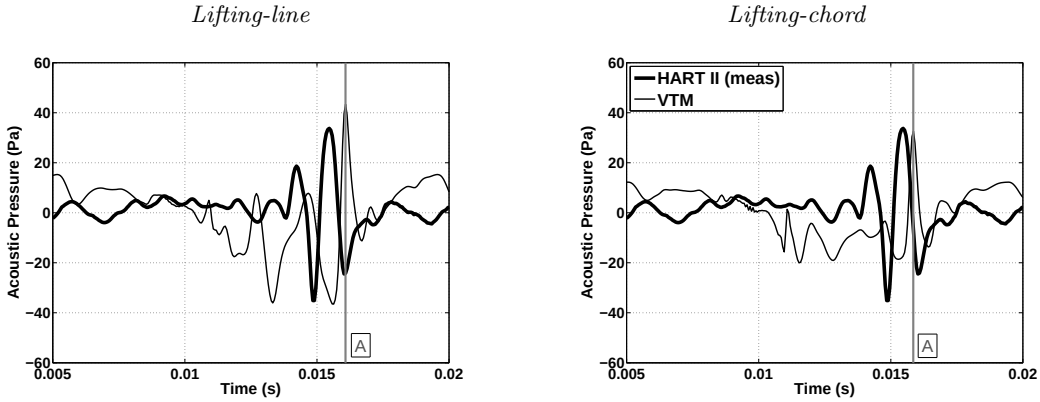

(a) *Time history of acoustic pressure for a single blade passage*

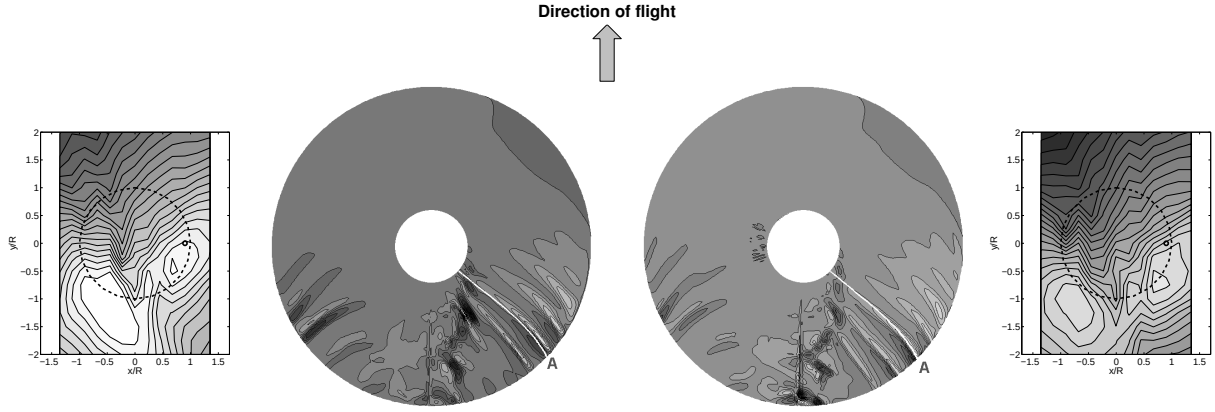

(b) *Predicted acoustic source density (loading noise, Pa/m^3)*

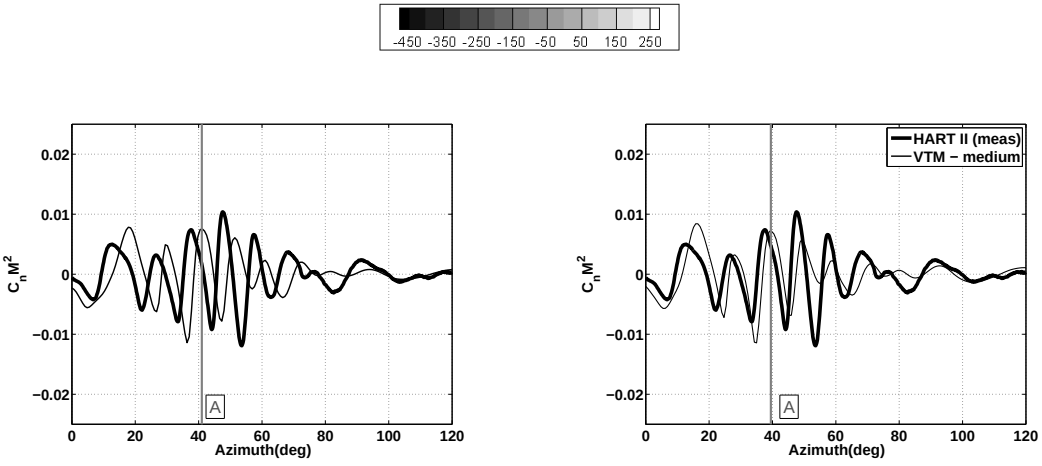

(c) *BVI-induced airloads*

Figure 15: *Time history of acoustic pressure for one blade passage and the corresponding BVI-induced airloads and source density distribution on the rotor for an observer located at the experimentally-measured SPL maximum on the advancing side of the rotor (HART II BL case). Numerical results are for the medium computational resolution.*

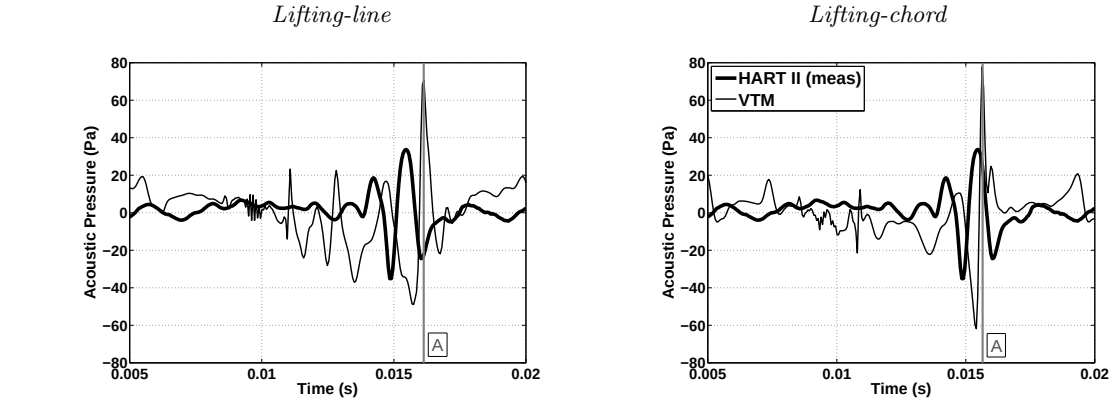

(a) *Time history of acoustic pressure for a single blade passage*

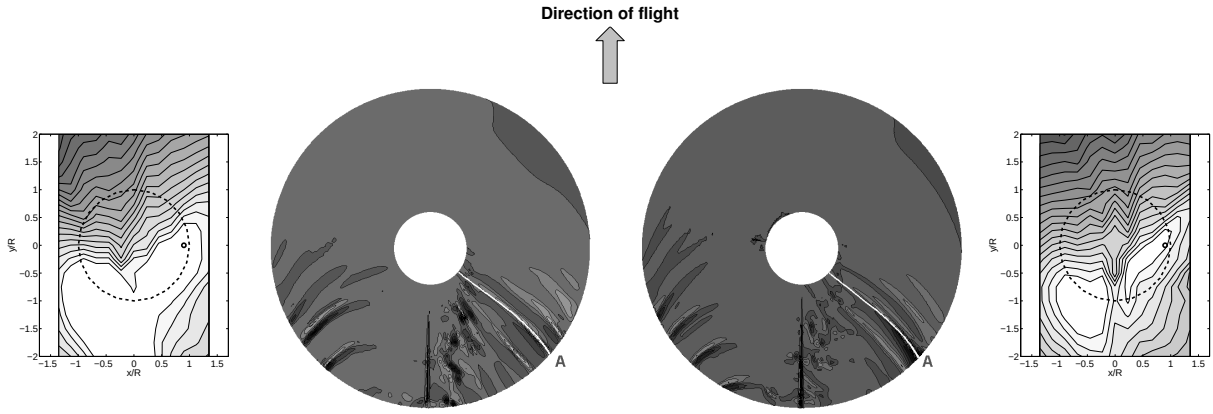

(b) *Predicted acoustic source density (loading noise, Pa/m^3)*

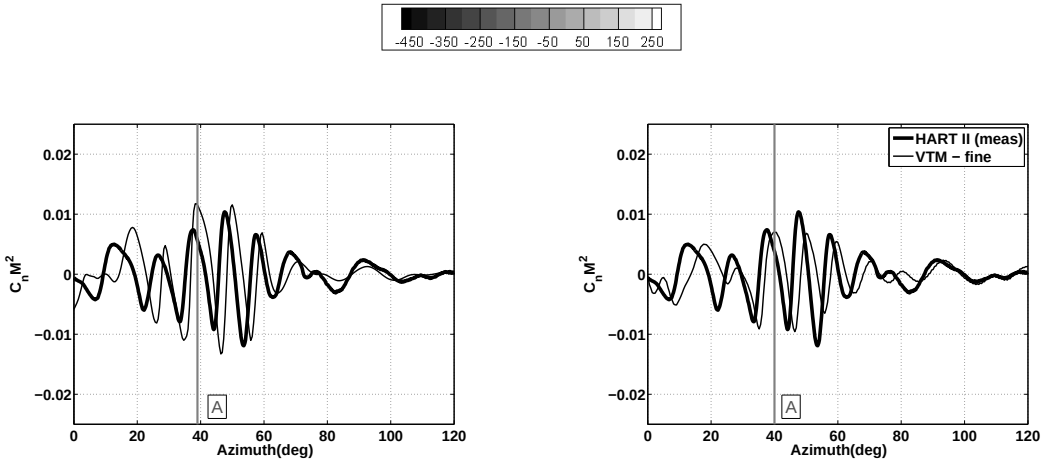

(c) *BVI-induced airloads*

Figure 16: *Time history of acoustic pressure for one blade passage and the corresponding BVI-induced airloads and source density distribution on the rotor for an observer located at the experimentally-measured SPL maximum on the advancing side of the rotor (HART II BL case). Numerical results are for the fine computational resolution.*

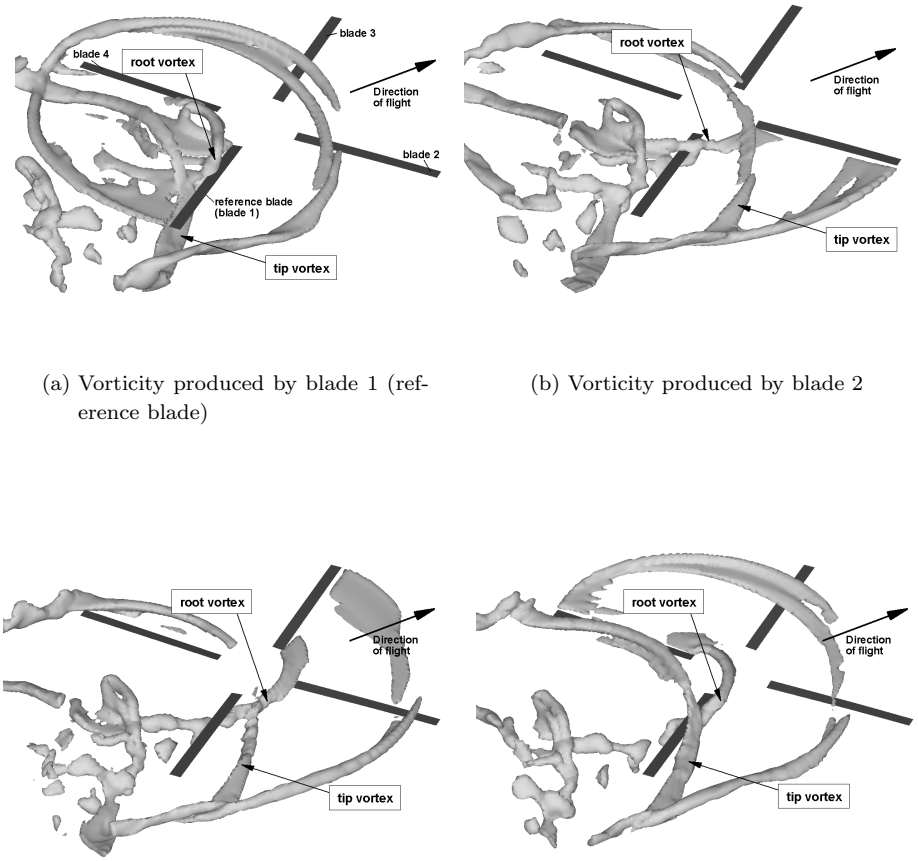

(a) Vorticity produced by blade 1 (reference blade)

(b) Vorticity produced by blade 2

(c) Vorticity produced by blade 3

(d) Vorticity produced by blade 4

Figure 17: *Geometry of the root and tip vortices as generated by each blade, when the reference blade lies at an azimuth of 40°.*

aerofoil theory. In this approach, the aerodynamic environment of the blade is represented by a series of weighted integrals over the chord of each blade panel. The version of the model that was used includes a prescription of the blade dynamics that is derived from the HART II experimental data.

The predicted airload for all three HART II flight case compares very favourably with the experimentally measured airloads. On the retreating side of the rotor, all BVI events discernible in the experimental data are reproduced by the numerics, usually with the correct phase. Generally on the advancing side of the rotor, the numerical resolution of the BVI-induced loads is less accurate both in amplitude and phase, yet all BVIs seen in the experimental data are still captured. For the MN and MV cases, both blade models have been shown to capture accurately the shifts in position of the BVI events on the rotor that result from the application of HHC.

Three computational resolutions were used to expose the effect of grid resolution on the quality of predictions. Where the lifting-line model was used to represent the aerodynamics of the blades, the predicted high-frequency, BVI-induced component of the loading is found to be extremely sensitive to the cell size that is used in the computations. The predicted amplitude of the BVI-induced features in the loading on the blades increases significantly as the cell size that is used to resolve the wake is reduced. A marked improvement in the accuracy of the predicted high-frequency airloads of the HART II rotor is obtained when a lifting-chord model for the blade aerodynamics is used instead of the lifting-line type approach. Errors in the amplitude and phase of the BVI-loading peaks are reduced and the quality of the prediction is affected to a lesser extent by the computational resolution. In particular, the over-prediction of the amplitude of the BVI events which occurs on the retreating side of the disc as the

resolution of the computation is increased when using the lifting-line model, is avoided.

The insensitivity of the lifting-chord model to the resolution of the computation can be explained in terms of its reduced sensitivity to the localised, small-scale features of the flow field and the dependence of its predictions rather on the integral, invariant properties of the flow field. In the context of helicopter BVI, the primary advantage of this approach would appear to be thus the possibility that it offers of true numerical convergence of predictions as the resolution of the computational grid is increased.

Similar conclusions extend to the predicted acoustic signature of the rotor. The experimentally-measured directivity of the radiated noise pattern is generally well captured by the numerics, as is the location and magnitude of the maxima in the sound pressure level on the ground plane below the rotor, at least on the retreating side of the disc. The upstream decay of the radiated signal is also well-captured, particularly in the BL test case. Yet again the larger deficiencies in prediction are encountered on the advancing side of the rotor, where magnitude and phase errors in the predicted BVI-induced component of the blade loading translate into more significant errors in the position and magnitude of the maximum in the sound pressure field on this side of the rotor than on the retreating side.

6 Acknowledgements

The authors would like to thank the members of the HART team for providing the data that was used in this study. In particular, the authors would like to thank Berend van der Wall and Joon Lim for their useful comments during the course of the research leading to this paper. The authors would also like to thank Jay Sitaraman and Karthik Duraisamy, authors of the acoustic post-processor used in this study.

7 References

1. van der Wall, B. G., Junker, B., Burley, C., Brooks, T., Yu, Y., Tung, C., Raffel, M., Richard, H., Wagner, W., Mercker, E., Pengel, K., Holthusen, H., Beaumier, P., and Delrieux, Y., "The HART II test in the LLF of the DNW - a Major Step towards Rotor Wake Understanding," *Proceedings of the 28th European Rotorcraft Forum*, Bristol, England, 2002.

2. van der Wall, B. G., Burley, C., Yu, Y., Richard, H., Pengel, K., and Beaumier, P., "The HART II test–Measurement of helicopter rotor wakes," *Aerospace Science and Technology*, Vol. 8, No. 4, 2004, pp. 273–284.

3. Lim, J., Tung, C., Yu, Y., Burley, C., Brooks, T., Boyd, D., van der Wall, B. G., Schneider, O., Richard, H., Raffel, M., Beaumier, P., Delrieux, Y., Pengel, K., and Mercker, E., "HART II: Prediction of Blade-Vortex Interaction Loading," *Proceedings of the 29th European Rotorcraft Forum*, Friedrichshafen, Germany, 2003.

4. Yu, Y., Tung, C., van der Wall, B. G., Pausder, H., Burley, C., Brooks, T., Beaumier, P., Delrieux, Y., Mercker, E., and Pengel, K., "The HART-II Test: Rotor Wakes and Aeroacoustics with Higher-Harmonic Pitch Control (HHC) Inputs – The Joint German/French/Dutch/US Project," *Proceedings of the American Helicopter Society 58th Annual Forum*, Montreal, Canada, 2002.

5. Boyd, D. D., "HART II Acoustic Predictions using a Coupled CFD/CSD Method," *Proceedings of the American Helicopter Society 65th Annual Forum*, Grapevine, TX, USA, 2009.

6. Lim, J., Nygaard, T., Strawn, R., and Potsdam, M., "BVI airloads prediction using CFD/CSD loose coupling," *Proceedings of the American Helicopter Society Annual Forum, Vertical Lift Design Conference*, 2006.

7. Lim, J. W. and Strawn, R. C., "Prediction of HART II Rotor BVI Loading and Wake System Using CFD/CSD Loose Coupling," *Proceedings of the 45th AIAA Aerospace Sciences Meeting and Exhibit*, Paper AIAA-2007-1281, Reno, NV, USA.

8. Whitehouse, G., Boschitsch, A., Quackenbush, T., Wachspress, D., and Brown, R. E., "Novel Eulerian Vorticity Transport Wake Module for Rotorcraft Flow Analysis," *Proceedings of the American Helicopter Society 63rd Annual Forum*, Virginia Beach, VA, USA, 2007.

9. Kelly, M. E., Duraisamy, K., and Brown, R. E., "Predicting Blade Vortex Interaction, Airloads and Acoustics using the Vorticity Transport Model," *Proceedings of the American Helicopter Society 9th Aeromechanics Specialist Meeting*, San Francisco, CA, USA, 2008.

10. Kelly, M. E. and Brown, R. E., "Predicting the wake structure of the HART II rotor using the Vorticity Transport Model," *Proceedings of the European Rotorcraft Forum*, Liverpool, UK, 2008.

11. Kelly, M. E. and Brown, R. E., "The effect of blade aerodynamic modelling on the prediction of high-frequency rotor airloads," *Proceedings of the American Helicopter Society 65th Annual Forum*, Grapevine, TX, USA, 2009.

12. Brown, R. E. and Line, A., "Efficient High-Resolution Wake Modelling using the Vorticity Transport Model," *AIAA Journal*, Vol. 43, No. 7, 2005, pp. 1434–1443.

13. Brown, R. E., "Rotor Wake Modeling for Flight Dynamic Simulation of Helicopters," *AIAA Journal*, Vol. 38, No. 1, 2000, pp. 57–63.

14. Toro, E. F., "A Weighted Average Flux Method for Hyperbolic Conservation Laws," *Proceedings of the Royal Society of London, Series A: Mathematical and Physical Sciences*, Vol. 423, 1989, pp. 401–418.

15. Peters, D., Hsieh, M.-C., and Torrero, A., "A state-space airloads theory for flexible airfoils," *Journal of the American Helicopter Society*, Vol. 52, No. 4, 2007, pp. 318–328.

16. Kenyon, A. R. and Brown, R. E., "Wake Dynamics and Rotor–Fuselage Aerodynamic Interactions ," *Journal of the American Helicopter Society*, Vol. 54, 2009.

17. Schneider, O., "Analysis of SPR measurements from HART II," *Aerospace Science and Technology*, Vol. 9, No. 5, 2005, pp. 409–420.

18. Schneider, O., van der Wall, B. G., and Pengel, K., "HART II Blade Motion Measured by Stereo Pattern Recognition (SPR)," *Proceedings of the American Helicopter Society 59th Annual Forum*, Phoenix, AZ, USA, 2003.

19. Pengel, K., Müller, R., and van der Wall, B. G., "Stereo Pattern Recognition – the technique for reliable rotor blade deformation and twist measurement," *Proceedings of the American Helicopter Society International Meeting on Advanced Rotorcraft Technology and Life Saving Activities (Heli Japan)*, Tochigi, Utsunomiya, Japan, 2002.

20. Farassat, F. and Succi, G. P., "A review of propeller discrete frequency noise prediction technology with emphasis on two current methods for time domain calculations," *Journal of Sound and Vibration*, Vol. 71, No. 3, 1980, pp. 399–419.